63-3-1

FTD-TT- 62-1252

TRANSLATION

TRANSACTIONS OF THE SEMINAR ON HEAT-RESISTANT MATERIALS
(SELECTED ARTICLES)

FOREIGN TECHNOLOGY DIVISION

AIR FORCE SYSTEMS COMMAND

WRIGHT-PATTERSON AIR FORCE BASE

OHIO

UNEDITED ROUGH DRAFT TRANSLATION

TRANSACTIONS OF THE SEMINAR ON HEAT-RESISTANT MATERIALS (SELECTED ARTICLES)

English Pages: 76

SOURCE: Russian Book, Trudy Seminara Po Zharostoykim Materialam, Nr. 4, Izdatel'stvo Akademii Nauk Ukrainskoy SSR, Kiev, 1959, pp. 38-51, 52-64, 96-107, 108-115.

PREPARED BY:

TRANSLATION SERVICES BRANCH
FOREIGN TECHNOLOGY DIVISION
WP-AFB, OHIO.

TABLE OF CONTENTS

AN INVESTIGATION OF WETTING OF THE SOLID SURFACES OF CERTAIN HIGH-MELTING COMPOUNDS BY MOLTEN METALS

V.N. Yeremenko and Yu.V. Naydich
(Institute of Metalloceramics and Special Alloys of the Acad. Sci. UkrSSR)

Introduction

A metalloceramic solid or cermet usually incorporates hard, high-melting ceramic components – oxides, carbides, and borides – with a metallic component which acts as a cementing binder. When the cermet is being prepared (sintering in the presence of a liquid phase or impregnation), this cement is in the liquid state.

The properties and production technology of metalloceramic substances are determined to a major degree by the wettability of the ceramic surface by the liquid metal [1]; it is this that suggests the necessity of detailed study of the qualitative laws governing the wetting.

Together with studying the general nature of the process (influence of temperature and time), the present paper investigates the relationship between wettability and other properties of the materials in the pair coming into contact.

General Qualitative Laws

The extent of wetting may be characterized by the wetting angle θ formed by the surface of the liquid where it meets the solid surface

(Fig. 1). The wetting angle is determined by the Neyman equation:

$$\cos\theta = \frac{\sigma_t - \sigma_{tzh}}{\sigma_{zh}}, \qquad (1)$$

where σ_t, σ_{tzh} and σ_{zh} are the specific free surface energies at the solid/gas, solid/liquid and liquid/gas phase boundaries, respectively.

Analysis of Eq. (1) shows that satisfaction of the following inequality [4] is a necessary condition for wetting (i.e., a small θ):

Fig. 1. Equilibrium of liquid drop on surface of solid. 1) σ_{tzh}; 2) σ_{zh}; 3) σ_t.

$$\sigma_{tzh} < \sigma_t \qquad (2)$$

In this case, wetting is determined by the interphase energy σ_{tzh}: the smaller this energy, the smaller will be the wetting angle and the better the wetting.

As we know, high-melting oxide materials are, as a rule, very seldom wetted by a liquid metal. For example, BeO and alundum are wetted by liquid aluminum (qualitative observations; wetting angle not known) [2]. Alundum is also wetted by tin, which [3] possesses good affinity for oxide surfaces. Veyl [Weil] [3] accounts for these data by assuming that metals capable of forming heavily charged ions (Sn^{+4}, Al^{+3}) should wet ceramic surfaces better because of the purely electrostatic interaction. Bondi [4] offered a different explanation for these phenomena. He assumed that the tin reduces a surface layer of the oxide to the metal. And metal is, as we know, thoroughly wetted by a metal. In our opinion, this explanation is not entirely correct, but it is rather important in that it suggests a chemical aspect of the wetting process.

A large quantity of experimental data on wetting of oxide materials enabled Kingery et al [5-9] to conclude that good wetting is impossible in the systems described unless a chemical reaction takes

place between the metal and the oxide. They established the rule (admittedly on the basis of a small number of examples) that those metals that have the greatest affinity to oxygen will wet oxides better.

The authors of [3-9] do not differentiate between chemical reaction and simple physical forces (polarization, dispersion) acting between the metal and the oxide. In the opinion of Bondi [4] and other authors [10], the chief obstacle to wetting of oxides by liquid metals is the high surface energy of liquid metal (1000 – 1500 ergs/cm) and the small surface energy of the oxides (in this case, Condition (2) is not satisfied).

It was ascertained later, however (on the basis of theoretical and experimental estimates of the surface energies of solids), that oxides have surface energies of the same order of magnitude as the metals.

The real reason for the unwettability of oxides [11] consists in the electronegativity of the oxide surface due to the large oxygen ions, which have negative charges and therefore repel electrons of the peripheral metallic atoms. The result is a large σ_{tzh} and, consequently, poor wetting.

Little is known concerning the wettability of carbides by liquid metals. It may be assumed that since the properties of carbide phases come closest to those of the metals, they should be wetted more easily by metals (since metal wets metal). However, this is not always the case.

It is known that certain metals, such as copper, zinc, tin and bismuth [11, 14], do not exhibit wetting and form wetting angles of the order of 100 – 120°. On the other hand, other metals (nickel, cobalt) rapidly impregnate the carbide skeleton.

We do not have data available on the wetting of borides by metals.

The Oxide-Metal System. Study of Relationship Between Properties of Oxide and its Wettability by Liquid Metal

As we have already noted, the condition $\sigma_{zh} \leq \sigma_t$ is approximately observed for oxides. However, the cause of the poor wettability of oxides is the high interphase energy σ_{tzh}, which is determined by the difference between the nature and structure of the phases in contact and must be smaller in those cases when these phases have closely similar properties. This premise is frequently justified in experiment: As a rule, metals wet metals (i.e., σ_{tzh} is small), silicates wet silicates, salts are wetted by fused salts, and organic crystals by nonpolar liquids. For two phases of different polarity, the interphase surface tension will be the smaller the smaller the difference between the polarities of these phases (Rebinder polarity rule).

The metallic oxides that are usually used in preparing a cermet are ionic compounds that possess semiconductor properties. Their electrical conductivity is determined by the number of charge carriers and depends little on their mobility [12, 13].

In ordinary nondegenerate semiconductors, the electron (or hole) concentration is considerably lower than in metals under the same conditions, and this, it seems to us, is responsible to a major degree for the differences between the properties of the semiconductor and the metal, since the characteristic properties of metals are determined precisely by the presence of a considerable concentration of electron gas (free electrons). Consequently, semiconductors with a large content of free charge carriers come closer to metals as regards their properties and should be wetted better by the metals.

However, σ_{tzh} diminishes with increasing rate of reaction between the metallic and oxide phases. At the present time, a relationship between conductivity and the adsorbing ability of the crystal has been

established [15]. The essence of this relationship consists in the following: free charges on the surface of the semiconductor crystal form unsaturated valences, and these are what effect transfer of current. Consequently, the activity of the semiconductor should increase with increasing conductivity.

The two premises given above have served as a point of departure for selecting a property of the solid phase that can be connected with wettability of the oxide by liquid metal. The conductivity (or number of charge carriers) of the oxide was found to be such a property.

The relationship between the wettability and conductivity of oxides was studied in the following manner.

Variable-composition oxides of the following systems were selected as solids having different conductivities in combination with other properties that were as closely similar as possible: MgO-NiO; MgO-CoO; Al_2O_3-Cr_2O_3; $MgO \cdot Cr_2O_3$-Fe_3O_4.

Each of these systems forms continuous series of solid solutions. In these systems, conductivity increases sharply (by five to seven orders) from left to right.

Tin (analytical grade), silver (99.99% Ag), nickel (99.99% Ni) and Armco iron were taken as the metallic phases.

Wetting was evaluated on the basis of the wetting-angle cosine ($\cos \theta$), which was determined by the reposing-drop method. The investigation was made in a vacuum or in an atmosphere of purified inert gas in a specially designed apparatus (Fig. 2) that enabled us to produce a vacuum of 10^{-6} to 10^{-5} mm Hg at a temperature of 1700°.

The ceramic specimens were prepared by pressforming mixtures of the powdered oxides with the cement and sintering at a temperature of 1750°. The specimen shape was a disc 25 mm in diameter and 5 mm thick. Data on the conductivity of the (Mg(Co)O and (Al, Cr)$_2O_3$ systems were

taken from Reference [16], and those for the $MgO \cdot Cr_2O_3 - Fe_3O_4$ system from Reference [17].

We measure the conductivity of the (Mg, Ni)O system by the method described in [16].

Table 1 presents the conditions under which wetting was investigated for different combinations of metalloceramic substances with • metals.

For each such combination, we constructed cos θ as a function of base composition at a specified temperature and as a function of temperature and time. The results that we obtained for wetting were compared with data on conductivity (Figs. 3-8).

The experiment showed that wetting increases symbatically with increasing conductivity for all of the systems investigated, while the wetting angles vary rather sharply – e.g., for the MgO-NiO-Sn system, θ drops from 130 to 10-20°.

Thus, the experiments carried out confirm the hypothesis of the existence of a relationship for oxides between conductivity and molten-metal wettability: As conductivity increases (with retention of crystal-lattice structure), wettability also increases. On the basis of the experiments carried out and literature data, we may draw certain conclusions as to the mechanism by which metals wet the oxide surface.

Let us first determine the nature of the forces acting on the metal/oxide interface.

The forces that can, in general, act between two regions are classified as physical and chemical. The physical interaction takes place instantaneously and is observed at all temperatures. The rates of the chemical interactions vary sharply with temperature.

The experiments showed that chemical forces play a decisive role in wetting phenomena involving substances with high surface energies

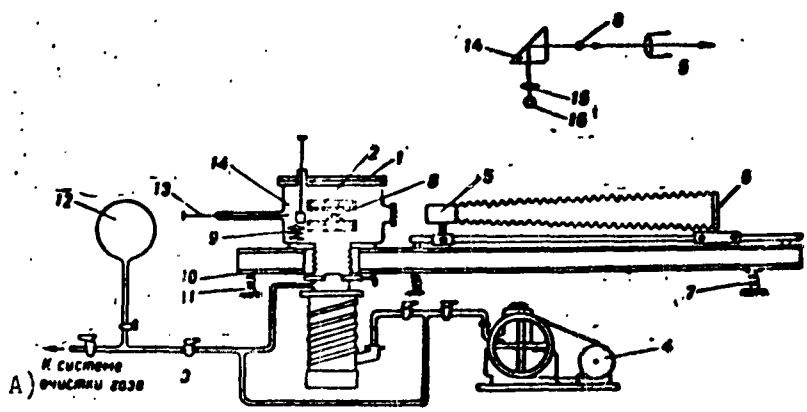

Fig. 2. Diagram of apparatus for investigation of wetting.
1) Vacuum chamber; 2) furnace; 3) oil-vapor pump with 500 liter/sec output; 4) forevacuum pump; 5) lens; 6) cartridge unit; 7) spring; 8) test specimen; 9) specimens for investigation; 10) bellows; 11) vacuum valve; 12) flask (inert-gas reservoir); 13) rod for changing specimens in furnace; 14) prism for rotating source beam; 15) condenser; 16) light bulb.
A) To gas-purification system.

TABLE 1.

1) Система	t, °C	2) Среда	3) Давление, мм рт. ст.
MgO — NiO — Sn	700—1000	4) Вакуум	$2 \cdot 10^{-5}$
MgO — NiO — Ag	1000—1300	5) Аргон	70
MgO — NiO — Cu	1000—1300	»	70
$MgO \cdot Cr_2O_3 - Fe_3O_4 - Sn$	700—1000	»	70
MgO — CoO — Sn	700—1000	4) Вакуум	6) около 10^{-5}
MgO — CoO — Ni	1500	5) Аргон	70
$Al_2O_3 - Cr_2O_3 - Fe$	1560	»	70

1) System; 2) medium; 3) pressure, mm Hg; 4) vacuum; 5) argon; 6) about 10^{-5}.

(high-melting metals and oxides). Below we shall set forth experimental data that demonstrate this statement.

1. The surface energy of the interface between the metal and the oxide is of the order of 10^3 ergs/cm^2 (see, for example, [8]).

Expressing this quantity in kilocalories per mole, we obtain the molar free surface energy. For this purpose, it is necessary to

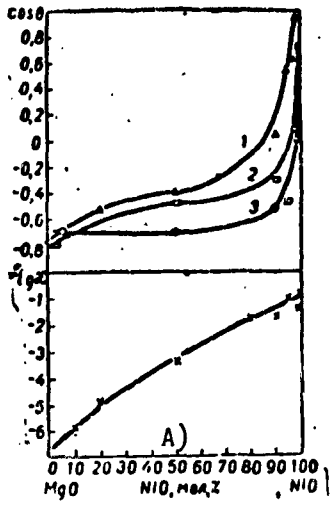

Fig. 3. Curves of wettability cos θ and conductivity (x) of MgO-NiO system: 1) Tin, temperature 1000°, vacuum (1 to 2) 10^{-5} mm Hg; 2) copper, temperature 1100°, argon, 70 mm Hg; 3) silver, temperature 1100°, argon, 70 mm Hg. A) NiO, mole-per cent.

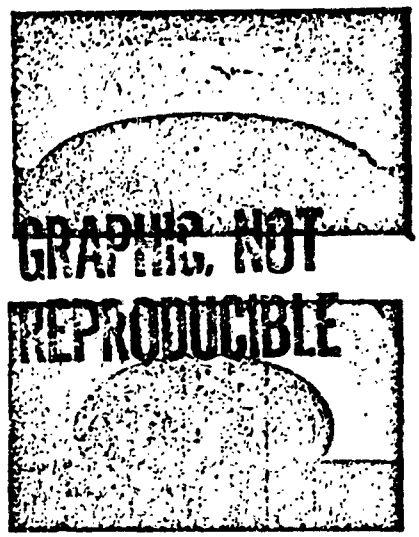

Fig. 4. Outline of molten tin drop on surface of magnesium oxide (1) and on surface of 99% NiO + 1% MgO (2).

multiply the specific surface energy by the area of one mole, assuming that the mole of material forms a monatomic layer:

$$\sigma_{мол} = \sigma_{уд} S_A N = \sigma_{уд} \left(\frac{M}{\rho}\right)^{\frac{2}{3}} N^{\frac{1}{3}} K,$$

where S_a is the area occupied by an atom or molecule, M is the molecular weight, ρ is the density, N is Avogadro's number, and K is the packing coefficient, which is near unity [19].

Carried out in this way, the calculation gives a value of the order of a few tens of kilocalories per mole for σ_{mol} (for MnO, σ_{mol} = = 50 kcal/mole). To cause any essential change in this quantity, it is necessary that the same energy be liberated in the reaction. Obviously, even though the physical forces are operating, they cannot significantly influence the interphase surface tension in the case under consideration, since the energy is only a few kilocalories per mole.

2. Experiment shows that the wetting angles of liquid metals

diminished, as a rule, with increasing temperature, assuming constant equilibrium values at each temperature.

The wetting angle is determined by the interphase energies.

As we know, surface energy diminishes with increasing temperature (the temperature coefficient is about 0.1 erg/°C). This change is minor and cannot account for the large decrease in the wetting angle as observed in experiments. Furthermore, at $\theta > 90^{\circ}$, assuming that all of the quantities σ_t, σ_{tzh} and σ_{zh} have the same temperature coefficient, we would observe an increase rather than a decrease in wetting angle. Obviously, the decrease in wetting angle can be accounted for only by a sharp drop in σ_{tzh}.

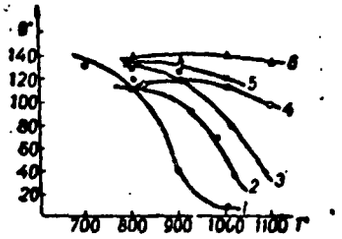

Fig. 5. Wetting angle of liquid tin on bases formed by the MgO-NiO system as a function of temperature for different quantities of MgO:
1) 1%; 2) 5%; 3) 10%;
4) 50%; 5) 80%;
6) 100%.

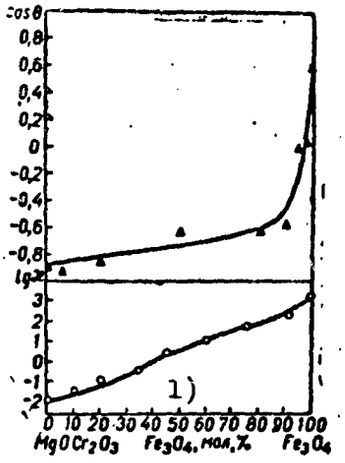

Fig. 6. Wettability and conductivity curves of $MgO \cdot Cr_2O_3$-Fe_3O_4 system at temperature of 1000° in argon atmosphere.
1) Fe_3O_4, mole-per cent.

We shall assume that a chemical reaction accompanied by a decrease in free energy takes place between the liquid metal and the solid base, in the surface layer. A certain quantity of free energy is liberated in each atomic event forming a chemical compound — chemical adsorption of an atom. The greater the number of metal atoms adsorbed on the oxide surface, the larger will be the energy

given off by the metal/oxide interface and the smaller the interphase surface tension.

An equilibrium is established at each temperature between the quantities of initial reagents and final reaction products, i.e., between the numbers of chemically adsorbed and desorbed atoms.

Consequently, a certain free-energy level is established for each temperature. In the present case, this takes place at the interphase boundary, which means that a certain value of σ_{tzh} is established.

The equilibrium proportions of the initial reagents and final products of the chemical reaction are determined by its equilibrium constant.

If the reaction is endothermic, the equilibrium constant increases with temperature and the system's free-energy reserve diminishes, i.e., σ_{tzh} also diminishes. It is just such an endothermic reaction, as will be shown later, that is usually observed in practice, and most experimental data have been derived for such reactions.

3. It has been established in experiment that the wetting angles of molten metals vary in time, diminishing and approaching a certain constant value (Fig. 9).

This fact is also easily explained if we assume that equilibrium is established at a finite rate in the chemical reaction and that this rate is given by the laws of reaction kinetics.

Consequently, σ_{tzh} and θ will change, diminishing and approaching an equilibrium value.

4. This also accounts for the dependence of wetting angle on the affinity of the molten metal to the oxygen of the solid oxide. As the affinity rises, the equilibrium constant will increase and the interphase energy will diminish.

5. As will be shown below, the relationship between wetting and

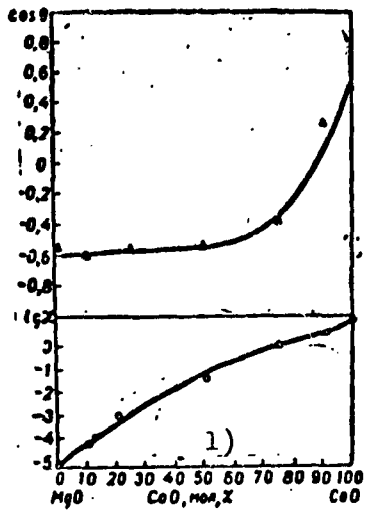

Fig. 7. Wettability and conductivity of MgO-CoO-Ni system at temperature of 1500° in argon atmosphere.
1) CoO, mole-per cent.

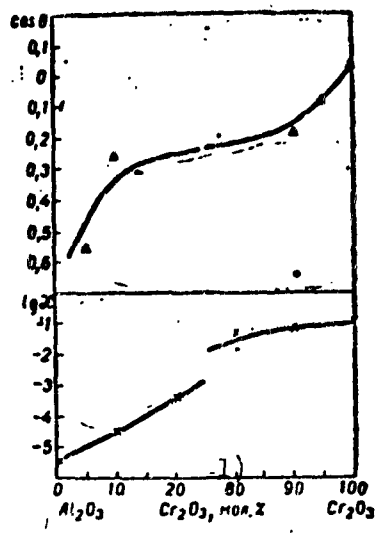

Fig. 8. Wettability and conductivity of Al_2O_3-Cr_2O_3-Fe system at temperature of 1550° in argon atmosphere.
1) Cr_2O_3, mole-per cent.

conductivity of oxides as observed in our experiments can be accounted for on a similar basis.

It is clear from the above that when the solid surface of an oxide is wetted by a liquid metal, a chemical reaction takes place. Using the premises developed in the electronic theory of adsorption on ionic semiconductive crystals [15], we may represent the microscopic picture as follows.

At a temperature of absolute zero and given an ideal lattice, an oxide consists of metal and oxygen ions having the structure of the corresponding inert gases (closed electron shells). The radius of the oxygen ion considerably exceeds that of the metal ion. We note that under these conditions, the electronic conductivity of the crystal is zero.

Let us examine the manner in which an electropositive atom (i.e., an atom of the metal) will react with the oxide surface. In this case,

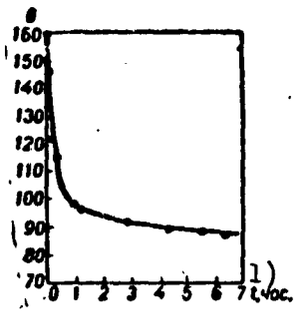

Fig. 9. Typical time curve of wetting angle, UO_2; copper + + 40% Al; 1100° [11].
1) t, hours.

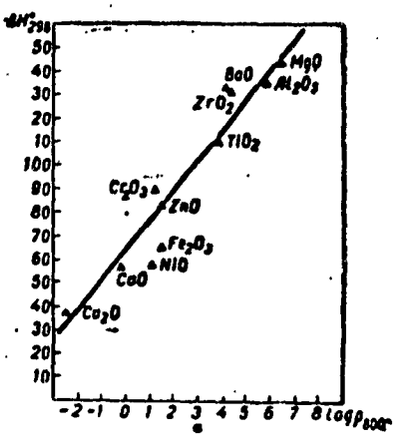

Fig. 10. Relationship between heat of formation and conductivity of oxides.

the reaction of the atom with the oxygen ions will be decisive, since the latter are always closer to the metallic atom. The metallic ions are, as it were, screened by the oxygen [11]. Obviously, no bonding forces can arise under these conditions (except for a weak physical interaction).

Let us now raise the temperature. As a result of the thermal motion in the crystal, the following disturbances will take place: an electron from an oxygen ion O^- will be returned to a metallic ion to form an oxygen ion O^{--} having a vacant position for an electron, or a hole. Both the electron and the hole can travel through the crystal, thus carrying current. A certain equilibrium number of such electrons and holes is established for each temperature; this can be computed by the formula

$$n = n_0 e^{-\frac{u}{kT}}, \qquad (3)$$

where u is the activation energy.

The oxygen ion O^- that has formed on the surface of the crystal (the hole) has a positive valence. Obviously, a metal atom that has approached the surface can fill the vacant position with its electrons

and form an ionic bond with the oxygen of the oxide.

The following reaction takes place:

$$Me'_2O + Me'' \rightleftarrows Me' \cdot Me''O + Me',$$

where Me' is the metal of the oxide; Me'' is the metal reacting with the oxide (for simplicity and clarity in the reasoning, we shall assume that the metal of the oxide and the metal reacting with the oxide are monovalent).

As the temperature rises (or as the number of lattice defects or impurity atoms increases), the number of free electrons and holes increases. The probability that an atom of the metal will combine with an available oxygen ion also increases.

The quantity u in Eq. (3) represents the height of the potential barrier crossed when an electron moves from an oxygen ion to an ion of the oxide metal. On the other hand, the process of oxide formation is accompanied by transfer of an electron in the opposite direction, contributing to liberation of an energy ΔH which is characteristic of the oxide's stability. Obviously, the quantities u and ΔH are interrelated and may vary symbatically. In fact, our comparison of experimental conductivity data with ΔH for the oxides approximately confirms this relationship (Fig. 10). This means that the more stable the oxide (i.e., the larger ΔH and u), the more difficult will be the process of local dissociation, the smaller will be the number of free charges and the conductivity of such an oxide at a given temperature, and the smaller will be the number of free valences at its surface.

Such a crystal must obviously have a lower activity and, consequently, lower wettability.

The qualitative reasoning presented above on the chemical interaction may be presented as a calculation of the interphase surface energy; this will lead to better understanding of the process mechanism.

TABLE 2.

1) Состояние	2) Концентрация			
	[Me'O]	[Me']	[Me"O]	[Me']
3) Начальное (I)	1	1	0	0
4) Промежуточное (II) . .	1—α	1—α	α	α
5) Равновесное (III.) . . .	1—α_0	1—α_0	α_0	α_0

1) State; 2) concentration; 3) initial (I); 4) intermediate (II); 5) equilibrium (III).

Let us first compute the free-energy margin of the system in which the chemical reaction is taking place. We shall make the calculation for a definite form of reaction equation:

$$Me'O + Me'' \rightleftarrows Me''O + Me', \tag{4}$$

i.e., for a case in which 1 mole of oxide reacts with 1 mole of metal. The equilibrium constant will obviously be written as follows:

$$K = \frac{[Me''O][Me']}{[Me'O][Me'']}.$$

The concentrations of the reagents in the initial, intermediate, and equilibrium states are listed in Table 2.

Provided that an infinitesimally small amount of the initial substances participates in the process (and, consequently, that an infinitesimally small amount of the final products is formed), the work of the reaction in the case of transition from state II to state III will be expressed as follows:

$$\frac{dZ}{d\alpha} = RT \ln \frac{\alpha^2}{(1-\alpha)^2} - RT \ln \frac{\alpha_0^2}{(1-\alpha_0)^2}. \tag{5}$$

On the other hand, the total work of the reaction in moving the system from state I to state III will be written as follows:

$$\Delta Z = \int_0^{\alpha_0} \frac{dZ}{d\alpha} d\alpha. \tag{6}$$

Denoting the respective isobar potentials for single moles of the initial substances Me'_0 and Me'' by Z' and Z'', we write the free energy of the system after equilibrium has been established in it:

$$Z = Z' + Z'' + \Delta Z \quad (\Delta Z < 0).$$

Taking the integral in Eq. (6), we obtain

$$\Delta Z = 2RT \ln (1 - \alpha_0)^0.$$

Knowing the standard variation of the isobar potential for the reaction (4), we may find the equilibrium concentration:

$$\Delta Z^0 = -RT \ln \frac{\alpha_0^2}{(1-\alpha_0)^3}.$$

For an endothermic reaction, α_0 increases with temperature, ΔZ assumes increasingly large negative values, and Z diminishes.

Let us now compute the interphase energy.

We shall regard the oxide surface as an ideal atomic plane on which monatomic chemical adsorption of the metal takes place; here, only those atoms of the oxides that are in its first superficial plane participate in the reaction.

Let us determine the number of moles of Me'O and Me'' that can be placed on one cm^2 of metal/oxide interface if they are stretched out into monatomic films.

We obtain as a result of the calculation

$$n' = \frac{1}{K' \left(\frac{M'}{\rho'}\right)^{\frac{2}{3}} N^{\frac{1}{3}}}; \quad n'' = \frac{1}{K'' \left(\frac{M''}{\rho''}\right)^{\frac{2}{3}} N^{\frac{1}{3}}},$$

where the prime ' refers to the oxide and the " to the metal. The respective denominators of these fractions are the areas occupied by the moles of Me'O and Me''. The initial value of the free energy per unit area of the two surfaces, i.e., the initial free-energy level of the interface (without taking physical interaction into account) will be

$$\sigma_{Me'O} + \sigma_{Me''}.$$

Then we obtain for $\sigma_{Me'O/Me''}$

$$\sigma_{Me'O} + \sigma_{Me''} + \Delta Z.$$

In this case, the initial quantities of reagents are n' and n''. Taking this into account, we obtain the following expression for ΔZ:

$$\Delta Z = RT\left[n' \ln\left(1 - \frac{\alpha_0}{n'}\right) + n'' \ln\left(1 - \frac{\alpha_0}{n''}\right)\right]. \qquad (7)$$

We note that the same expression is obtained for ΔZ as before for n' = = n'' = 1.

The value of α_0 is determined from the equation

$$\Delta Z^0 = -RT \ln \frac{\alpha_0^2}{(n' - \alpha_0)(n'' - \alpha_0)},$$

where $\frac{\alpha^2}{(n' - \alpha_0)(n'' - \alpha_0)}$ is the equilibrium constant taking into account the fact that the initial concentrations of the reagents are n' and n''. The quantity ΔZ^0 may obviously be found as follows:

$$\Delta Z^0 = \Delta Z^{0''} - \Delta Z^{0'},$$

where $\Delta Z^{0'}$ and $\Delta Z^{0''}$ are the standard free energies of formation of the oxides for the metals Me' and Me''.

In practice, the hard oxide is usually more stable than the oxide of the wetting metal in preparation of a cermet or in the conduct of wetting experiments. This means that $\Delta H^0 = \Delta H^{0''} - \Delta Z^{0'}$ is a positive quantity, i.e., that the reaction is endothermic. It follows from this that as the temperature rises, the equilibrium constant and α_0 increase and σ_{tzh} diminishes.

Analysis of Formula (7) shows that it accounts for the following experimental relationships: 1) the drop in σ_{tzh} with temperature; 2) the drop in σ_{tzh} with increasing affinity of the liquid metal to oxygen; 3) the drop in σ_{tzh} with increasing conductivity of the hard oxide (with increasing conductivity, $\Delta H'_0$ and $\Delta Z'_0$ diminished).

With diminishing $\Delta Z^{0'}$, on the other hand, the equilibrium constant

of the reaction (4) increases and σ_{tzh} declines.

The formula considered does not enable us to obtain numerical values for the interphase energy, since it contains the unknown quantity σ_t. However, the wetting angle may be computed from it, as is required in practice.

The quantity ΔZ is the work of adhesion. In fact, we obtain by the Dupre equation

$$\sigma_{TM} = \sigma_T + \sigma_M - W_A,$$
$$\sigma_{TM} = \sigma_T + \sigma_M + \Delta Z,$$

and obviously

$$\Delta Z = -W_A.$$

But $W_A = \sigma_{zh}(1 + \cos\theta)$; this is what defines the wetting angle.

An estimate calculation that we carried out for certain metal/oxide pairs indicates that the orders of magnitude obtained are correct. It is apparently not possible to expect greater accuracy from such an approximation. The theory requires further perfection and refinement.

Carbide/Metal System. Relationship Between Wetting and Properties of Metallic Phase

No special investigations of wetting in the carbide/metal system were carried out. Here we shall analyze only experimental available in the literature, refining certain wetting-angle values and supplying new ones.

Metals can be classified into two large groups in accordance with their ability to wet a carbide surface.

1. Metals that interact weakly with the carbide surface (Table 3). These metals produce large wetting angles on the carbide surface and do not spread out even at high temperatures.

2. Metals that interact vigorously with the carbides. These

TABLE 3.

1) Система	t, °C	θ°	2) Атмосфера	3) Литература
Ni — WC	200—500	160—700	4) Аргон	[11]
Sn — WC	500—1300	120—30	»	»
Bi — WC	500—1200	150—30	»	»
Cu — TiC	1100—1300	108—70	5) Вакуум	»
Cu — ZrC	1100—1700	140—118	4) Аргон	»
Pb — TiC	400—1000	152—90	»	»
Ag — TiC	980	108	5) Вакуум	»
Al — TiC	700	118	»	[14]
Zn — TiC	550	120	»	[14]

1) System; 2) atmosphere; 3) literature; 4) argon; 5) vacuum.

spread out flat over the carbide surface, penetrating the carbide-grain framework thoroughly. According to our data, these include nickel, cobalt and iron. These metals dissolve carbides, forming eutectic-type equilibrium diagrams with them (with TiC) [17].

Chromium, titanium, molybdenum, niobium and zirconium should also be included in this group /18/.

On analyzing the cause of this difference in the wetting properties for the two groups of metals, we note that metals of the first group have completed (or vacant) d-shells, i.e., they are nontransitional.

On the other hand, metals with defects in the d-shell, which fall into the second group, react vigorously with carbides and wet their surfaces thoroughly. It follows from this that when carbides are wetted by metals, the s-d-interaction plays a decisive role and that only transitional metals can wet carbides efficiently.

The same qualitative laws should apparently be observed for other phases as well — borides and nitrides.

Boride-metal System. Comparison of the Wettability of Borides with Their Other Properties

We studied the wettability of hot-pressed borides* by copper in

the temperature range from 1100 to 1400° as a function of holding time.

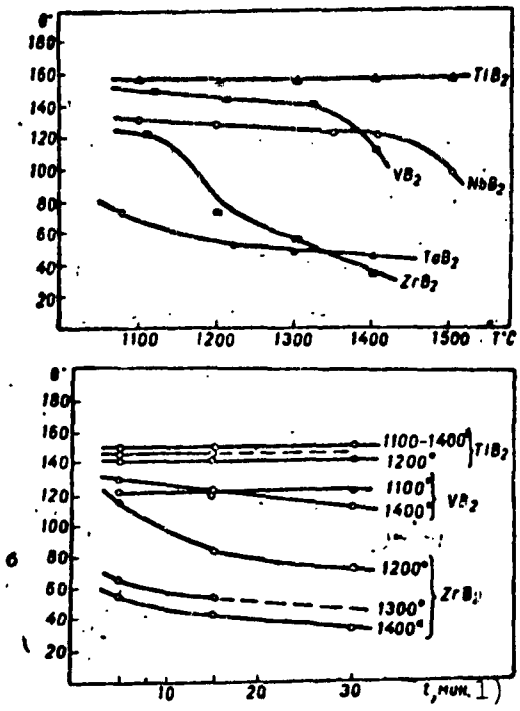

Fig. 11. Wetting angle of liquid copper on boride surfaces as a function of temperature (a) and as a function of holding time (b). 1) t, min.

The specimens were polished on emery wheels with progressively decreasing abrasive-grain sizes and were then washed with gasoline and alcohol prior to the investigation. The experiments were conducted in an atmosphere of purified argon. The results are presented in Fig. 11.

As we see, wettability varies very sharply, increasing in the following sequence (at temperatures from 1100 to 1300°):

$$TiB_2 \rightarrow VB_2 \rightarrow NbB_2 \rightarrow ZrB_2 \rightarrow TaB_2$$

It will be seen from the diagrams of wetting angle as a function of temperature (Fig. 11a) that there exists for each compound a certain temperature above which we observe a sharp decrease in the wetting angle; below this temperature, the wetting angle varies only very slightly even with time.

We made approximate determinations of the wetting temperatures of the borides and obtained the following values: $TiB_2 > 1500°$; $NbB_2 \sim 1450°$; $VB_2 \sim 1300 - 1350°$; $ZrB_2 \sim$ ...[illegible] $- 1150°$; $TaB_2 < 1100°$.

Above these temperatures, the wetting angle varies rapidly in time, and below them it is not a function of time. It follows from

comparison of the wetting angles in the temperature range from 1100 to 1300° with the properties of the borides investigated that wettability increases with increasing atomic number of the transitional metal forming the boride (group IV of the periodic system: θ = 158° for TiB_2, θ = 60° for ZrB_2; group V of the periodic system: θ = 145° for VB_2, θ = 125° for NbB_2, θ = 50° for TaB_2). The strength of the bond between the metal and boron atoms diminishes simultaneously.

Levy and Murray [11] found that the wettability of carbides increases with increasing ratio r_{nemet}/r_{met}, i.e., with diminishing radius of the metallic atom. This relationship is not observed in the case of the borides.

It must be noted in conclusion that the conceptions developed for the chemical interaction in the case of the oxides and the calculation of the interphase energy are also valid for carbide/metal and boride/metal systems, although the wetting mechanism is, of course, different in this case and the reaction takes place in accordance with a different equation.

Conclusions

1. An apparatus for investigation of the wetting process was designed and built.

2. The wettability of the hard-oxide/liquid-metal system was studied.

It was found in accordance with the hypothesis advanced that the wettability of oxides increases with conductivity and that oxides with high conductivities are thoroughly wetted by liquid metals. An explanation was given for wetting processes and a calculation of the interphase surface energy was carried through.

3. Wettability in the carbide/metal system was analyzed. The hypothesis that wetting in these systems is determined by s-d-

interaction was advanced.

4. The wettability of borides by liquid copper was studied. Wettability was compared with other properties of the borides.

REFERENCES

1. W.D. Kingery, J. Amer. Cer. Soc., 36, 362, 1953.
2. Z.O. Olsen, J. Appl. Phys., 16, 425, 1945.
3. W.A. Weyl, J. Soc. Glass Techn., 33, 220, 1949.
4. A. Bondi, Chem. Rev., 52, 417, 1953.
5. Economons, W. Kingery, J. Am. Cer. Soc., 36, 403, 1953.
6. M. Humenik, W. Kingery, J. Am. Cer. Soc., 37, 18, 1954.
7. W. Kingery, M. Humenik, J. Phys. Chem., 67, 3, 1953.
8. W. Kingery, J. Am. Cer. Soc., 37, 42, 1954.
9. C. Kurngian, W. Kingery, J. Phys. Chem., 60, 94, 1956.
10. L. Williams, P. Murray, "Metallurgya", 49, 210, 1954.
11. D. Lievey, P. Murray, Warmfeste und Korrozionbestaendige Sinterwerkstoffe [Corrosion-resistant Sintering Materials with High Hot Strength], 2nd Plansee Seminar, Reutte, Tirol, 1956.
12. A.F. Ioffe, Poluprovodniki v sovremennoy fizike [Semiconductors in Modern Physics], Izd-vo AN SSSR (Acad. Sci. USSR Press), 1954.
13. B.G. Kolomiyets and N.A. Goryunova, Voprosy teorii i issledovaniya poluprovodnikov i protsessov poluprovodnikovoy metallurgii [Problems of Theory and Research in Semiconductors and Processes of Semiconductor Metallurgy], Izd-vo AN SSSR, 1955.
14. A.I. Belyayev and Ye.A. Zhemchuzhniy, Poverkhnostnyye yavleniya v metallurgicheskikh protsessakh [Surface Phenomena in Metallurgical Processes], Metallurgizdat [State Press for Literature on Metallurgy], 1952.
15. Problemy kinetiki i kataliza [Problems of Kinetics and Catalysis], Issue VIII, Elektronyye yavleniya pri katalize i adsorbtsii

[Electronic Phenomena in Catalysis and Adsorption], Izd-vo AN SSSR, 1955.

16. V.N. Yeremenko and A.M. Beynish, ZhNKh [J. Inorganic Chemistry], 1, 9, 1956.

17. V.N. Yeremenko, ZhNKh, 1, 9, 1956.

18. W. Kingery, F.A. Halden, Am. Cer. Soc. Bull., 36, 117, 1955.

19. A. Skapski, A. Metallurgica, 4, 6, 1956.

•

[Footnotes]

Manuscript Page No.	
15	$\ln(1 - \alpha_0) < 0$, since $\ln \alpha_0 < 1$; with increasing α_0, ΔZ becomes increasingly large in absolute magnitude, retaining its negative sign.
17	The authors express their gratitude to G.V. Samsonov for the boride specimens that he provided.

[List of Transliterated Symbols]

Manuscript Page No.	
2	т = t = tverdyy = solid
2	ж = zh = zhidkiy = liquid
20	неmет = nemet = nemetallicheskiy = nonmetallic
20	мет = met = metallicheskiy = metallic

MAXIMUM GAS-BUBBLE PRESSURE METHOD AS APPLIED TO DETERMINATION OF SURFACE TENSION OF METALS OF THE IRON FAMILY

V.V. Fesenko and V.N. Yeremenko
(Institute of Metalloceramics and Special Alloys of the Acad. Sci. UkrSSR)

Among the existing methods for measuring the surface tension of metals and high temperatures at the liquid-gas interface, the maximum-gas-bubble pressure method offers certain advantages. It is based on measurement of the maximum pressure in the bubble that forms in the passage of a capillary tube lowered into the molten metal. The influence of impurities in measurements made by this method is reduced to a minimum, since each successive measurement is made on a freshly formed surface.

The method is experimentally simple and comparatively well-elaborated theoretically; this makes it possible to use it for measuring surface tension on many metals and alloys at temperatures above 1000°.

Among the disadvantages of the method, we should note the difficulty of preparing the capillaries, which must not react with the molten metal, and the absence of a general computational method, since the mechanism of formation and breakaway of the bubble has not been adequately studied for the case of failure of the molten metal to wet the capillary material.

Theory of the Method

The maximum-pressure method was proposed by Simon in 1851. Kantor (1892) elaborated the theory of bubble formation. Schroedinger [1] gave an exact equation for computing surface tension. The technique was brought to its culmination by Sugden [2], who developed a method for computing surface tension by use of the Bashforth and Adams tables, while Sauerwald et al [3] used it extensively for determining the surface tension of a number of metals and alloys. Subsequently, the surface tensions of metals and alloys were determined by this method in many studies [4, 5].

Like certain other methods for determining the surface tension of fluids, the maximum-pressure method is based on utilization of the Laplace capillarity equation (1806), which describes the shape of the interface between two phases at equilibrium under the action of the forces of surface tension and gravity. For any surface, this equation takes the form

$$\sigma\left(\frac{1}{R_1}+R_2\right)=c+gz(D-d) \qquad (1)$$

or, for the case of maximum pressure,

$$P=c+gz(D-d), \qquad (2)$$

where σ is the surface tension at the boundary between two phases with densities D and d; R_1 and R_2 are the principal radii of curvature of the surface at the point in question, z is the coordinate of this point reckoned along the vertical from the peak of the bubble, c is a constant equal to the pressure difference between the convex and concave sides of the bubble, g is the acceleration of gravity and P is the equilibrium gas pressure inside the bubble.

Since the density of one phase (the metal) is considerably higher than that of the other phase (gas), the latter may henceforth be dis-

regarded.

Figure 1 shows the stages in formation of a bubble blown from a quite narrow capillary tube given complete wetting of the tube material by the liquid.

When the capillary is immersed into the liquid, the latter rises through the tube to a definite height (position 1).

When gas is admitted to the capillary, the meniscus undergoes no change in shape as it is pushed downward through the tube until it reaches position 2. As the pressure rises, the meniscus turns into a bubble (position 3); then the pressure increases until the bubble has acquired a hemispherical shape (position 4).

If additional gas is admitted into the capillary, the bubble begins to swell rapidly, the pressure in it drops, and it breaks.

According to (1), the pressure maximum in the bubble corresponds to the minimum of its radius of curvature, i.e., to the conditions under which the radius of curvature of the bubble is equal to the radius of the tube ($R_1 = R_2 = r$, where r is the capillary radius).* The maximum pressure, which is governed in this case only by capillary forces, is equal to the pressure difference between the convex and concave sides of the bubble. For this case, Eq. (1) will take the form

$$P = 2\sigma/r. \qquad (3)$$

Equation (3) is normally known as the Kantor equation.

If we express P in terms of the equivalent height of the liquid being investigated [$h = (P/g)D$] and remember that the capillary constant $a^2 = rh$, we obtain

$$a^2 = \frac{2\sigma}{gD}. \qquad (4)$$

Equation (4) is applicable for computing surface tension only in cases where the spherical-bubble condition is satisfied, i.e., where

the capillary is extremely narrow or the surface tension is very large (r/a small).

For wider capillaries, when the bubble shape deviates from the spherical (r/a = 0.2), the Schroedinger formula

$$a^2 = rh\left(1 - \frac{2r}{3h} - \frac{r^2}{6h}\right). \qquad (5)$$

is applicable.

In the case of larger values of r/a (up to 1.5), the surface tension should be computed by the Sugden method, which employed the results of the extremely close approximate integration of the capillarity equation as obtained by Bashforth and Adams [6]. These authors reduced Eq. (1) to the form

$$\frac{1}{R/b} + \frac{\sin\varphi}{x/b} = 2 + \beta\frac{z}{b}. \qquad (6)$$

This can be done as follows.

The constant c in Eq. (1) is determined from equality of the principal radii of curvature at the apex of the bubble, i.e., from the expression

$$c = \frac{2\sigma}{b};\ R_1 = R_2 = b,\ z = 0,$$

where b is the radius of curvature at the apex of the bubble.

As we see from Fig. 2, R = x/sin φ. Substituting the values of c and R_2 in (1), we obtain

$$\sigma\left(\frac{1}{R_1} + \frac{\sin\varphi}{x}\right) = \frac{2\sigma}{b} + gDz. \qquad (7)$$

Dividing all terms of this equation by σ/b and adopting the notation

$$\beta = \frac{Db^2g}{\sigma}, \qquad (8)$$

we obtain Eq. (6), in which each term is a dimensionless quantity, β determines the shape of the bubble, and b determines its size (scale). Setting b = 1 on an arbitrary scale, we obtain

$$\frac{1}{R} + \frac{\sin\varphi}{x} = 2 + \beta z. \qquad (9)$$

Bashforth and Adams integrated this equation, expanding 1/R, sin φ/x and z in series in powers of φ.* These authors compiled the detailed tables of values of x/b and z/b for various values of β and φ.

Replacing the pressure in Eq. (2) by the equivalent height of the liquid being studied and applying (4), we obtain the equation used by Sugden as a point of departure:

$$h = \frac{a^2}{b} + z$$

or

$$\frac{hr}{a^2} = \frac{r}{b} + \frac{r}{a}\cdot\frac{z}{b}\cdot\frac{b}{a}. \qquad (10)$$

where r is the inside radius of the tube.

The problem is solved by finding the value Y that satisfies the condition

$$a^2 = Yh. \qquad (11)$$

We find from Eqs. (8), (10) and (11) that

$$\frac{r}{Y} = \frac{hr}{a^2} = \frac{r}{b} + \frac{r}{a}\cdot\frac{z}{b}\sqrt{\beta/2}. \qquad (12)$$

Each value of r/b is computed as follows:

$$\frac{r}{b} = \frac{r}{a}\cdot\frac{a}{b} = \frac{r}{a}\sqrt{2\beta}. \qquad (13)$$

Since the value r/b corresponds to the x/b from the Bashforth-Adams tables, we may, on determining it for any value of r/a for various values of β, take from the tables the φ and z/b that correspond to it, and then substitute z/b in (12) and determine r/Y.

As the pressure in the bubble rises, the quantity r/Y passes through a maximum. Sugden computed a series of minimum values of Y/r for r/a = 0 to 1.50 and compiled a table by means of which it is possible to compute the surface tension at the liquid-gas interface

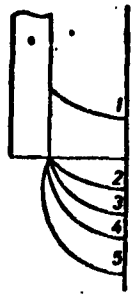

Fig. 1. Stages in formation of bubble assuming that liquid wets material of capillary.

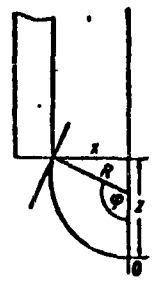

Fig. 2. Diagram showing formation of bubble after Sugden ($\theta < 90^\circ$).

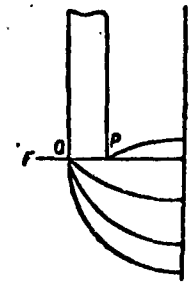

Fig. 3. Diagram of bubble formation after Sauerwald and Draht ($\theta > 90^\circ$).

with extremely high accuracy using broad capillaries.

Up to this point, we have been considering the case of complete wetting of the capillary tube by the liquid under investigation, i.e., $\theta = 0$, and all calculations have been made taking the inside radius of the tube into account.

In measuring the surface tensions of metals, the tube normally used is ceramic and not wetted by the melt ($\theta > 90^\circ$).

It is customary to assume that the wetting angle is a minor factor in measurements by the maximum-pressure method. If $\theta < 90^\circ$ (the liquid wets the face of the capillary), the calculation must be made with the inside radius; if $\theta > 90^\circ$ (the liquid retreats to the outer margin of the tube) it must be carried out with the outside radius [7].

In 1928, Sauerwald and Draht [8] measured the surface tensions of a number of metals with glass and quartz capillaries, computing the data from the outside radius. As will be seen from Fig. 3, the boundary of the surface at the instant when the meniscus changes from convex to concave shifts to the outer edge of the capillary, where the bubble passes through the same stages as in the case of full wetting, the only difference being that the bubble grows on the outer face of

the tube and the calculations are made using the outside diameter.

In spite of the fact that the Sauerwald-Draht diagram describes a particular case of bubble formation, as will be shown below, it was used and is still used by many investigators for determining surface tensions in cases where $\theta > 90^{\circ}$.

As long ago as 1930, Porter showed that this diagram is not applicable in the general case [9]. Using the Poisson-Rayleigh equation,* he computed the pressure necessary to move the meniscus through several stages from the inside to the outside edge of the tube at a constant wetting angle of the fluid against the capillary material. The calculation showed that, depending on the size of the passage and the thickness of the capillary walls, the pressure will be at its maximum at either the position C or E (Fig. 4).

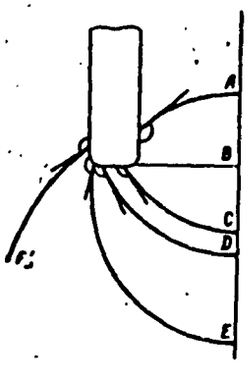

Fig. 4. Diagram of bubble formation after Porter ($\theta > 90^{\circ}$).

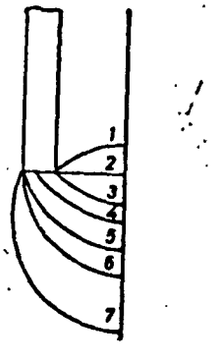

Fig. 5. Diagram of bubble formation after Levin ($\theta > 90^{\circ}$).

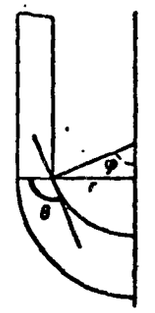

Fig. 6. Diagram of bubble formation with $\theta > 90^{\circ}$.

Porter obtained by theoretical derivation a graphical representation of the pressure due to surface tension as a function of bubble radius at wetting angles of 90, 120, 135 and 150°.

Using this relationship, we may vary the thickness of the capillary walls in such a way that the maximum pressure will always correspond to formation of the bubble at the outer perimeter.

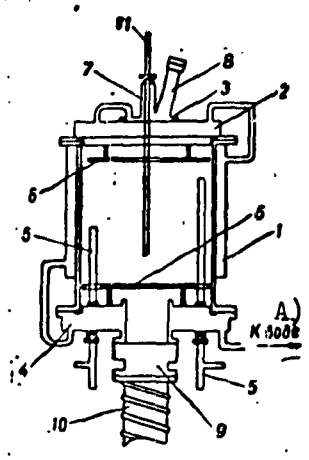

Fig. 7. Vacuum chamber:
1) Housing;
2) large upper cover; 3) small upper cover;
4) lower cover;
5) current lead-ins; 6) nickel screens; 7) capillary packing;
8) inspection window; 9) vacuum lock; 10) TsVL-100 vapor-jet pump.
A) To water.

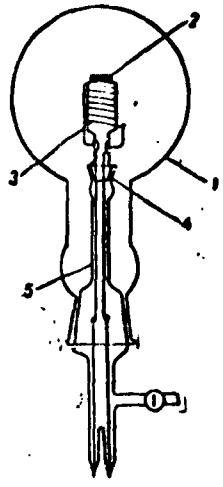

Fig. 8. System for purification of gases:
1) Flask; 2) steel cup with calcium;
3) quartz plug with tungsten winding; 4) unlubricated ground joint;
5) glass rod with ground joint and molybdenum lead-ins.

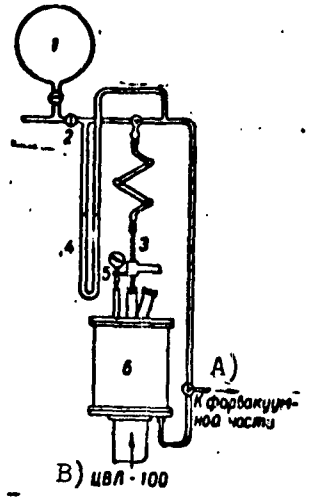

Fig. 9. Diagram of apparatus for measuring surface tension by maximum-bubble-pressure method:
1) Gas collector;
2) regulating valve;
3) capillary tube;
4) oil manometer;
5) adjustable fixture with indicator;
6) chamber.
A) To forevacuum unit; B) TsVL-100.

Figure 5 presents a diagram of bubble formation according to Levin [11, 12]. Levin considered extremely narrow capillaries (no deviation of bubble shape from the spherical) with sharp edges, of the type ordinarily used in surface-tension measurements.

According to this diagram, the meniscus will flatten when gas is admitted into the tube and the bubble radius will then diminish from $r = r_\infty$ to $r = r_3$; then, as will be appreciated from Fig. 6, the bubble radius will be $r_3 = r/\sin\theta$, where r is the inside radius of the tube.*

In this position, the excess gas pressure in the bubble will be

$$P_s = \frac{2\sigma}{r}\sin\theta. \qquad (14)$$

On admission of additional gas into the tube, the bubble flattens out across the face of the tube, retaining the equilibrium wetting angle; here, the bubble radius first increases and the pressure in it drops (positions 4 and 5, Fig. 5), and then diminishes to become equal to the outside radius of the tube. The pressure at this point in time will be

$$P_6 = \frac{2\sigma}{R}. \tag{15}$$

where R is the outside radius.

What happens after this will be the same as in the case of complete wetting.

Thus, according to both Levin and Porter, we should observe two pressure maxima: the first corresponding to position 3 in Fig. 5 (according to Porter, C in Fig. 4), and the second to position 6 (according to Porter, E in Fig. 4).

In surface-tension measurements by the maximum-pressure method, only one maximum is ordinarily observed. The radius at which the bubble is formed may be established from relationships (14) and (15). In fact,

$$P_6 > P_3$$

only provided that

$$R < \frac{r}{\sin\theta}. \tag{16}$$

It follows from (16) that as $\theta \to 180°$ for any capillary, the maximum pressure will correspond to formation of the bubble on the outside face of the tube, i.e., only in this case will the Sauerwald-Draht diagram be valid. Equation (16) which is analogous to the graphical condition of Porter (9), enables us to select a capillary such that the maximum pressure will correspond to formation of the

bubble on the outside perimeter of the capillary.

However, the ranges of application of the methods considered above are limited. The Porter method is applicable for values r/a = = 0.3 to 0.4,* while the Levin method, which is based on Eq. (3), is valid only for cases in which r/a → 0. Moreover, it is not always possible to vary the thickness of the capillary wall, particularly if the surface tension is being measured at high temperatures using beryllium-oxide or aluminum-oxide capillaries. The use of thin-walled quartz capillaries at temperatures above 1400° gives unreproducible results [12, 13].

It follows from the above that for cases in which $\theta > 90°$ and the observed maximum pressure does not correspond to formation of a bubble on the outside perimeter of the tube, the maximum gas-bubble pressure method is not suitable for measuring the surface tension of liquids, although it may be employed if a method for computing the surface tension is worked out to take the wetting angle into account for different values of r/a. However, the precision of such a method is lower because the size of the wetting angle will participate in the calculations, and this angle is determined relatively roughly, particularly at high temperatures.

To compute surface tension in this case, we employed the Sugden method with slight modifications.

Equation (13) may be written

$$r/a = \frac{r}{b}\sqrt{\beta/2}. \qquad (17)$$

Substituting the value of r/b into Eq. (17) from the Bashforth-Adams tables for a number of values of β and a given θ (or φ, since $\theta = 180 - \varphi$), we may compute a series of values of r/a. Substituting the resulting values of r/a and the r/b, z/b and β corresponding to

them into Eq. (12), we may obtain a number of values of r/Y for the given θ.

TABLE 1

β	r/b	z/b	r/a	Y/r
0,00	0,9397	0,6540	0,00	0,9397
0,125	0,9243	0,6383	0,231	0,9610
0,25	0,9103	0,6207	0,353	0,9878
0,5	0,8855	0,5404	0,443	1,0069

Suppose, for example, that $\theta = 110°$ ($\varphi = 70°$). Let us find the values of r/b and z/b for various β from the tables. We compute r/a from Eq. (17) for each β. Using Expression (12), we obtain Table 1.

The table is compiled in the same way up to values r/a = 0.5. Then, applying exact interpolation, we may construct a table of values of r/Y for r/a = 0 to 1.5 for any θ.

We compiled such tables for wetting angles of 100, 110, 120 and 130°. Using these tables for values of r/a and θ, the surface tension is determined as per Sugden, by successive approximations according to the formula

$$\sigma^2 = Yk.$$

This method of computing surface tension is applicable only for cases in which capillaries with thick walls and $\theta \neq 180°$ are used. For any other capillary and wetting angle, it is necessary to establish exactly whether the maximum pressure corresponds to bubble formation on the outer perimeter of the tube (for various values of r/a). This may be done by applying the Porter method, but, as we have already noted, the range of application of this method is highly restricted.* Consequently, for large values r/a, we employed a more general method consisting in the following.

In cases where the pressure maximum corresponds to formation of a bubble on the outside face of the tube, i.e., when the Sugden method is applicable, the pressure maximum is observed when Y/r is minimal.

Substituting for r in the Sugden table the values of the outside radius R of the tube, we determine the quantity Y_R for the given R/a and then determine the Y_θ corresponding to r/a from the tables that we have composed for the θ in question. Since the maximum pressure corresponds to the minimum radius of curvature, the condition with which the maximum pressure will correspond to formation of the bubble on the outside perimeter of the capillary will be written as follows:

$$Y_R < Y_\theta \qquad (18)$$

Consequently, if condition (18) is satisfied, the surface tension must be computed by the Sugden method, while if it is not satisfied, the wetting angle must be taken into account in the calculations, using the tables that we have compiled.

EXPERIMENTAL

1. Apparatus for Surface Tension Measurement by the Gas-Bubble Maximum-Pressure Method

The apparatus for the surface-tension measurements was designed in such a way that measurements could be made at high temperatures (up to 1800°) and contamination of the metal specimen would be minimized in the process. For this purpose, a tungsten-coil furnace was employed; melting of the metal and measurement of its surface tension took place in a vacuum in an atmosphere of protective gases [Fig. 7].

The covers and lead-ins were vacuum-sealed by means of rubber gaskets placed in special slots; the housing and covers were cooled by running water. The capillary used for the surface-tension measurement was secured in the removable upper cover in a Wilson-type packing [15, 16]. A vacuum was produced in the chamber with the aid of rotary (RVN-20) and vapor-jet (TsVL-100) pumps and was measured by thermocouple and ionization manometers.

The smelting furnace was a beryllium-oxide ceramic cylinder 10 cm high and 5.5 cm in inside diameter. A tungsten cable spun from six wires, each having a section of 0.2 mm, was mounted in channels inside this cylinder. The furnace was installed inside the chamber on two molybdenum spacers and provided with screens of nickel and molybdenum sheet. To protect the tungsten wire from spattering of metal, a beryllium-oxide crucible was set up in the furnace. This crucible accommodated the sheet-molybdenum inserts and the crucible in which the metal was melted. The current was fed to the winding by means of water-cooled leads. The temperature in the furnace ran up to 1800°. The heating current was regulated by means of an autotransformer (maximum current 25 amp at voltage of 100 to 120 v).

The temperature was registered and regulated by means of TsNIIChM-1 thermocouples and an electronic potentiometer to within $\pm$20°.

Beryllium-oxide capillary tubes with inside diameters from 0.3 to 0.4 cm were used to measure the surface tension. The capillaries were secured to quartz tubes by means of a putty consisting of water glass, beryllium oxide powder and aluminum oxide. During the experiments, the point of mounting was located inside the chamber near the top cover. Round-passage capillary tubes with uniform wall thicknesses were selected for the work and were polished thoroughly with fine emery paper. The dimensions of each capillary were measured under a microscope in four directions, after which the inside and outside diameters were determined as the averages from the four measurements.

Much attention was devoted to purification of the gases – hydrogen and helium – used to form the bubbles, since very small admixtures of nitrogen and particularly of oxygen in the gases may sharply reduce the metal's surface tension. A diagram of the gas-purification

procedure is shown in Fig. 8.

The quartz furnace with its tungsten winding was installed in a 6 – 7-liter flask, using a ground glass plug with molybdenum lead-ins. Metallic calcium was placed in this furnace in a steel cup. The winding was heated by a current controlled by the autotransformer.

A diagram of the apparatus for determining surface tension is presented in Fig. 9. The purified gas was collected in a gas collector from which it could enter the measurement tube through a regulating stopcock. The gas pressure in the tube was measured with a manometer filled with apiezon oil (oil density 0.894 g/cm^3). The accuracy of the manometer scale was 0.5 mm.

The measurement tube was connected with the glass part of the apparatus through bent tubes with six ground joints, which made it possible to shift the capillary tube vertically to more than 100 mm without breaking the vacuum in the system. A regulating device with a dial-type indicator was used in moving the measurement tube to get an accurate determination of the depth to which it was immersed into the metal; this device made it possible to determine the immersion depth to within 0.001 cm.

2. Technique of Surface-Tension Measurement

In the surface-tension measurements, 100 – 150 g of the metal was placed in the crucible and introduced into the furnace, where the crucible was entered. Then the capillary was inserted into the packing and the top cover placed on the chamber. Then using the ground joints, the capillary was connected with the glass part of the apparatus and the entire apparatus was evacuated by the vacuum pumps. When the vacuum in the chamber reached 10^{-6} mm Hg at room temperature, the furnace was slowly heated.

Since the vacuum in the chamber dropped on heating, the temperature

was not raised until that vacuum had reached $10^{-5} - 10^{-4}$ mm Hg. During this time, hydrogen at a pressure of about 0.5 atmosphere was pumped into the evacuated flask to purify the gases; it was kept in the flask for 1.5 – 2 hours over the calcium, which was heated to a temperature of 700 – 800°.

Then the purified hydrogen was collected in the gas collector; the purification flask was evacuated and helium admitted to it.

When the metal in the crucible had melted, the gas from the gas collector (or from the purification flask) was admitted to the measurement tube through the regulating stopcock; here, the forevacuum part of the system was disconnected from the tube by means of the communicating stopcock. Then the capillary was lowered slowly using the regulating device; at the instant when the metal surface came into contact with capillary tube, the manometer with the apiezon oil registered the pressure change. Then the tube was lowered to a certain depth and the maximum pressure determined (with the chamber being evacuated by the pumps at all times).

When a gas bubble raced through the molten metal, some of the metal was splashedonto the crucible, i.e., the immersion depth of the capillary tube changed. Consequently, the maximum pressure was measured several times with the capillary tube immersed to the same depth (at the same temperature). Then the immersion depth was measured and the pressure remeasured. The measurements were repeated five to six times for certain levels and temperatures.

3. Results of Tension Measurements on Metals

To check the method to be used for the surface-tension measurements, we first measuredthe surface tension of pure mercury and pure tin using the quartz capillaries.

The calculation was made by the Sugden method. For mercury at

room temperature, we obtained a surface-tension value of 476 ± 10 ergs/cm^2, which agrees with the generally accepted values (460 – 480 ergs/cm^2 [17 – 19]) within the limits of experimental error.

For tin at a temperature of 600°, we obtained a surface-tension value of 533 ± 7 ergs/cm^2; this also agrees with literature data [17, 20].

The experiments with mercury and tin indicated that the method was suitable for measurement of the surface tensions of metals, thus encouraging us to use it in surface-tension measurements on metals of the iron family.

Measurement of surface tension on iron-family metals

The literature contains almost no reliable data on the surface tensions of such pure metals as nickel, cobalt and iron.

TABLE 2

1 Подложка	2 Значение поверхностного натяжения в разных средах		
	3 Вакуум	4 Водород	5 Гелий
6 Двуокись тория	—	1540	1530
7 Двуокись циркония . . .	1730	1555	1500
8 Окись алюминия	1760	1590	1505
9 Окись бериллия	1680	1585	1370
10 Окись магния	1600	1730	1625
11 Двуокись титана	1165	1320	1110

1) Base; 2) suface-tension values in various media; 3) vacuum; 4) hydrogen; 5) helium; 6) thorium dioxide; 7) zirconium dioxide; 8) aluminum oxide; 9) beryllium oxide; 10) magnesium oxide; 11) titanium dioxide.

Despite the fact that the surface tension of pure iron has been investigated by many authors, the data obtained have been so contradictory that it is difficult even to adopt an order of magnitude. Thus, it was found quite recently that the surface tension of iron was 883 ergs/cm^2 and that it was 1850 ergs/cm^2 [21, 22].

The surface tension of nickel has been investigated only by

Kingery and Humenik, who used the reposing-drop method [23]. They observed that the surface tension of nickel was a function of the nature of the gas in which the measurements were made and of the base on which the nickle drop was placed. Table 2 presents values of the surface tension as obtained by Kingery and Humenik at a temperature of 1470°.

To the best of our knowledge, there are no literature data concerning the surface tension of cobalt.

Measurement of surface tension of nickel

Highly purified nickel (99.99% Ni) was used in the experiments to measure surface tension. Data on the density of liquid nickel were taken from Reference [24]. The values of the wetting angles of nickel on beryllium oxide and helium in hydrogen at a temperature of 1500 – 1700°, as obtained in measurement of the surface tension of nickel by the reposing-drop method [25], were 110°. For the maximum pressure to correspond to formation of a bubble on the outer face of the tube at this wetting angle, the capillary walls must be thinner than 0.02 cm (with a 0.2-cm inside radius of the tube). Since it is impossible to make a capillary with such a wall, the measurements were made with thicker-walled capillaries and the wetting angle was taken into account in the calculations.

The results of the experiments are listed in Table 3 (R = 0.316; r = 0.185).

As will be seen from this table, the surface tension of nickel is virtually independent of temperature, but it does depend on the medium.

The error in the surface tension determination is governed basically by the error of measurement of the wetting angle. We consider that a wetting angle measured with an error of 5° produces an

TABLE 3

h	t, °C	D	Среднее значение поверхностного натяжения 1	
			в атмосфере 2 гелия	в атмосфере 3 водорода
2,06	1500	7,76	1485	—
2,39	1530	7,69	—	1655
2,18	1600	7,53	1530	—
2.26	1700	7,34	1545	4

1) Average value of surface tension; 2) in helium atmosphere; 3) in hydrogen atmosphere.

error of $\pm$ 60 ergs/cm^2 in the value of surface tension for nickel.

Measurement of surface tension of cobalt

TABLE 4

R	r	h	Среднее значение поверхностного натяжения 1	
			в атмосфере 2 гелия	в атмосфере 3 водорода
0,328	0,188	2,12	—	1630
0,326	0,186	2,27	1620	1640

1) Average value of surface tension; 2) in helium atmosphere; 3) in hydrogen atmosphere.

We conducted measurements of surface tension for cobalt of high purity (99.99% Co). Since no data on the density of liquid cobalt have been published, we found this quantity experimentally. The surface tension was determined at a temperature of 1600°. The wetting-angle value for cobalt on beryllium oxide at the same temperature in atmospheres of hydrogen and helium was determined from photographs of drops [25]; it is 108 – 110°. Table 4 lists the results of surface-tension measurements for cobalt (D = 7.55). As in the case of nickel, the error in the surface-tension value for cobalt was $\pm$60 ergs/cm^2.

Measurement of surface tension of iron

For the surface-tension measurement, we used electrolytic iron (99.92% Fe; 0.02% Mn; 0.04% C; 0.01% Si) and iron produced by vacuum sublimation (99.99% (Fe + Ni); 0.03% Ni). The data on the density of liquid iron were those of [24]. The wetting-angle value for iron at a temperature of 1600° was 120° in both hydrogen and helium [25]. The wetting angle was taken into account in the calculations. Table 5 presents the results of measurements of the surface tension of iron at a temperature of 1650° (D = 7.1). In view of the fact that the wetting angle of iron on beryllium oxide is larger than that of nickel, the error in the surface-tension determination will also be large (±90 ergs/cm^2).

TABLE 5

Fe, %	R	r	A	Среднее значение поверхностного натяжения 1	
				в атмосфере 2 гелия	в атмосфере 3 водорода
99,99	0,311	0,185	2,00	1430	1400
99,92	0,327	0,187	1,76	1270	—
99,92	0,354	0,236	1,43	1280	—
99,92	0,339	0,221	1,5	—	1250

1) Average surface-tension value; 2) in helium atmosphere; 3) in hydrogen atmosphere.

RESULTS

1. A general method was developed for computing surface tension by the method of maximum gas bubble pressure, taking the wetting angle into account for cases where the liquid does not wet the interior of the capillary.

2. A vacuum apparatus was set up for determining the surface tension of metals by the maximum gas-bubble pressure method at high temperatures (to 1800°).

3. The surface tension of nickel was measured in helium at temperatures of 1500, 1600 and 1700°. The surface-tension value for nickel in this case is (1520 ± 60) ergs/cm^2 and is virtually independent of temperature. In hydrogen, the surface-tension values were higher by more than 100 ergs/cm^2.

4. The surface tension of cobalt was measured at 1600° in hydrogen and helium. It was shown that the surface tension of cobalt does not depend on the nature of the gas and is (1600 ± 60) ergs/cm^2.

5. The surface tensions of electrolytic iron and iron produced by vacuum sublimation were measured. The surface tension of iron does not depend on the nature of the gas at 1650° and the values obtained were, respectively, (1260 ± 90) and (1415 ± 90) ergs/cm^2.

REFERENCES

1. E. Schroedinger, Ann. d. Phys., [Annals of Physics], 46, 413, 1915.
2. S. Sugden, J. Chem. Soc., 858, 1922.
3. F. Sauerwald et al., Zs. anorg. allgem. Chem. [Journal of Inorganic and General Chemistry], 162, 301, 1927; 181, 353, 1929; 213, 310, 1933.
4. L.K. Kunin, Poverkhnostnyye yavleniya v metallakh [Surface Phenomena in Metals], Gostekhizdat [State Publishing House for Technical and Theoretical Literature], 1955.
5. V.K. Semenchenko, Poverkhnostnyye yavleniya v metallakh i splavakh [Surface Phenomena in Metals and Alloys], Gostekhizdat, 1957.
6. F. Bashforth, An attempt to test the theories of capillary action, Cambridge, 1883.
7. N.K. Adam, Fizika i khimiya poverkhnostey [Physics and Chemistry of Surfaces], Gostekhizdat, 1947.

8. F. Sauervald, J. Draht, Zs. anorg. Chem., B 154, 79, 1926.
9. A.W. Porter, Phys. Mag., 9, 1965, 1930.
10. Z. Rayleigh, Proc. Roy. Soc., A 92, 184, 1915.
11. A.M. Levin, Zavodskaya laboratoriya [Industrial Laboratory], 28, 1101, 1952.
12. A.M. Levin, Nauchnyye trudy Dnepropetrovskogo metallurgicheskogo instituta [Scientific Transactions of the Dnepropetrovsk Metallurgical Institute], Elektrometallurgiya [Electrometallurgy], 28, 95, 1952.
13. L.L. Kunin and O.A. Klyako, Zavodskaya laboratoriya, 6, 750, 1950.
14. A.N. Krylov, Lektsii o priblizhennykh vychisleniyakh [Lectures on Approximate Calculation], Gostekhizdat, 1954.
15. Vakuumnoye oborudovaniye i vakuumnaya tekhnika [Vacuum Equipment and Vacuum Technique], IL [Foreign Literature Press], 1951.
16. V.A. Lanis and L.Ye. Levina, Prakticheskiye osnovy vakuumnykh ispytaniy [Practical Foundations for Vacuum Tests], Gosenergoizdat [State Publishing House for Literature on Power Engineering], 1955.
17. Spravochnik khimika [Chemist's Handbook], Goskhimizdat [State Publishing House of Literature on Chemistry], Vol. 1, 1951.
18. P.P. Pugachevich, ZhETF [Journal of Experimental and Theoretical Physics], 17, 648, 1947.
19. P.P. Pugachevich and V.A. Konstantinov, DAN SSSR [Proceedings of the Academy of Sciences USSR], 57, 797, 1947.
20. N.L. Pokrovskiy and M. Saidov, Fizika metallov i metallovedeniy [Physics of Metals and Metallography], 2, 546, 1956.
21. T.P. Kolesnikova and A.M. Samarin, Izvestiya AN SSSR, OTN [Bulletin of the Academy of Sciences USSR, Division of Tech-

nical Sciences], 5, 63, 1956.

22. W. Esche, O. Peter Arch. Eisenhüttenwesen [Archives of Iron Metallurgy], 27, 353, 1956.

23. W.D. Kingery, M. Humenik, Phys. Chem., 57, 359, 1953.

24. C. Benedicks, N. Ericson. G. Ericson. Arch. Eisenhüttenwesen, 3, 473, 1930.

25. V.N. Yeremenko, V.I. Nizhenko and Yu.N. Ivashchenko, Metod lezhashchey kapli dlya izmereniya poverkhnostnogo natyazheniya metallov semeystva zheleza [Reposing-Drop Method for Measuring Surface Tension of Iron-Family Metals], see present collection.

Manuscript Page No.

[List of Transliterated Symbols]

35 ЦНИИЧМ = TsNIIChM = Tsentral'nyy nauchno-issledovatel'skoy institut chernoy metallurgii = Central scientific-research institute for ferrous metallurgy

Manuscript Page No.

[Footnotes]

25 In the case of narrow capillaries.

27 In the differential form, this equation may be written as the system of equations [14]:

$$\frac{dz}{d\varphi}=R_1\sin\varphi;\ \frac{dr}{d\varphi}=R_1\cos\varphi;\ \frac{1}{R_1}-\frac{\sin\varphi}{r}=2+\beta z$$

29 This equation is one of the approximate results of integration of the basic capillarity equation. It is applicable for r/a = 0.4 [10].

30 It is evident from Fig. 6 that sin $\varphi = r/r_3$ and $\theta = 180-\varphi$, whence $r_3 = r/\sin\theta$.

32 At r/a = 0.7, the error in using the Poisson-Rayleigh equation exceeds 1%.

33 The Levin method is useful only in the limiting case where $r/a \to 0$.

INFLUENCE OF ASH-FORMING COMPONENTS IN LIQUID FUEL

ON DETERIORATION OF GAS-TURBINE MATERIALS

Review

R. F. Mocharnyuk

(Institute of Metalloceramics and Special Alloys

Academy of Sciences UkrSSR)

Introduction

Alloys based on iron, cobalt, nickel and chromium with molybdenum, tungsten, niobium, vanadium and titanium additives are used as materials with high hot strength for gas turbines.

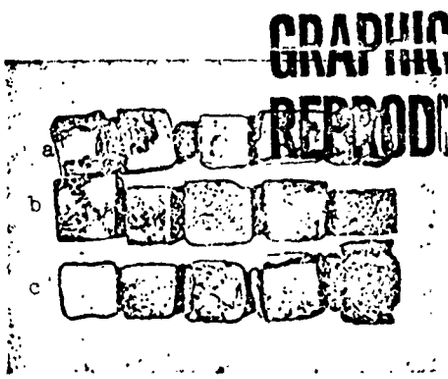

Fig. 1a. Oxidation of carbon steel (a), type 410 stainless steel (b) and a steel with 8% Cr and 2% Ni (c) at 890°.

Fig. 1b. Accelerated oxidation of steel with 8% Cr and 2% Ni.

The high-temperature corrosion resistance of these materials has been found quite satisfactory, since the basic alloys usually contained chromium.

The influence of large additives of such elements of molybdenum, tungsten, niobium and vanadium on the high-temperature corrosion

resistance of the alloys has so far been the object of relatively little study. Leslie and Fontana [1] showed, for example, that under certain conditions additives of molybdenum are detrimental: they produce severe oxidation of the alloy.

In view of the unusual behavior of these alloys at high temperatures, extensive investigations of their high-temperature corrosion resistance were initiated and resulted in observation of a special type of oxidation known in the literature as accelerated, fast or catastrophic oxidation. This oxidation was first observed only for pure tungsten [2], for molybdenum [3] and for molybdenum-containing alloys (16% Cr; 25% Ni; 6% Mo) [1].

The basic difference between accelerated oxidation and the oxidation usually observed among metals and alloys consists in the fact that the corrosion product (oxide film) that forms during accelerated oxidation is not a barrier to continuous breakdown of the metal. The oxide layers are either completely nonprotective (linear oxidation process) or cause by themselves more intensive breakdown as the oxidation rate and the thickness of the oxide layer increase.

Alloys that are predisposed to accelerated oxidation in air usually have vanadium, tungsten and molybdenum as additives (Figs. 1a and 1b).

The oxidation rate in the presence of such additives diminishes in the sequence from vanadium to molybdenum. A common property of these elements is the fact that their higher oxides have very low melting points and high vapor pressures. The melting points of the oxides also increase from vanadium to molybdenum.

Below a temperature of 710°, alloys containing vanadium, molybdenum or tungsten show normal oxidation; accelerated oxidation is observed only above a certain critical temperature, which depends

on several factors. This criti al temperature is highest for tungsten and lowest for vanadium.

The "Vanadium Problem"

It has been established experimentally that alloys that do not contain certain "harmful" elements will sometimes deteriorate if a substance containing these elements or compounds of them comes into contact with the surface being oxidized [5 – 11, 26].

These "harmful" destructive compounds include V_2O_5, Na_2O, CaO, Al_2O_3, Na_2SO_4 and others present in the ash of liquid fuel.

The "vanadium problem" has been developed extensively during recent years; this problem arises with the use of oils containing vanadium as fuels in gas turbines.

In addition to the normal products of hydrocarbon combustion, oxides of sulfur and inorganic ash form during combustion of the fuel and it is these products that produce most of the corrosion in turbine materials.

It is known that air corrosion of hot-strength alloys at high temperatures proceeds exceptionally rapidly under conditions in which the surface of the material is contaminated with certain low-melting components [10, 12]. Here the corrosion rate increases [13] and assumes catastrophic dimensions.

The corrosion rate exceeds 270 cm/year; this represents a serious danger for gas turbines, steam boilers and other installations where normal hot-strength alloys are subjected to attack by the hot gases produced in the combustion of certain petroleum grades containing traces of vanadium. Although there may be less than 0.01% of V in the fuel oil, over 50% of it concentrates in the ash of this oil. The ash particles usually move in the gas stream and build up on the metallic surfaces that they strike.

A vanadium-containing fuel produces an ash with a melting point of about 650°. In marine gas turbines, for example, the operating temperature is 650 – 700°, and the ash produced in the combustion chamber is carried out in the molten or liquid stage and absorbed on the turbine blades or the air-heating tubes.

The vanadium oxide that is stable in air at elevated temperatures is V_2O_5. Its melting point is very low (670°). It is known that mixtures of this oxide with certain metallic oxides have melting points depressed as low as 550°. Since the oxidation resistance of hot-strength alloys is related to the creation of a protective oxide barrier separating the metal from the corrosive environment, it becomes clear what the consequences will be if low-melting products form and are then washed from the surface (Fig. 2).

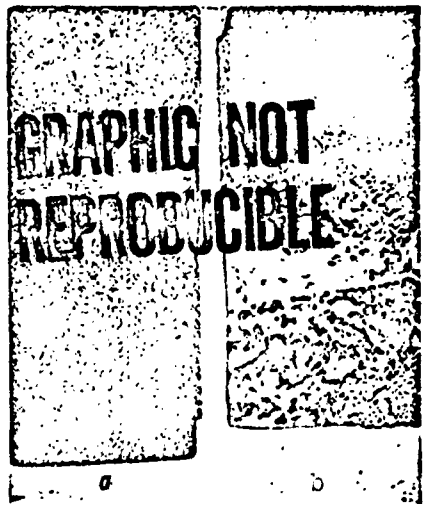

Fig. 2. Catastrophic oxidation of steel in molten vanadium oxide (V_2O_5) at liquidus line: a) Corrosion products removed; b) corrosion products not removed.

The "vanadium problem" first made its appearance in 1948 [32]. In recent years, a considerable amount of attention has been devoted to this problem, but it still remains basically unsolved.

Two theories were advanced to accounts for the high rates of corrosion. According to one of these, these rates are due to dissociation of the oxides V_2O_5, WO_3, and MoO_3 with formation of oxygen and oxides of lower valence [1]. According to the other theory, the low-melting higher oxides V_2O_5, WO_3 and MoO_3 accumulate on the working surface and react with oxides of the initial alloy to form low-melting coumpounds that are readily washed from the surface [4, 13, 14], which is what

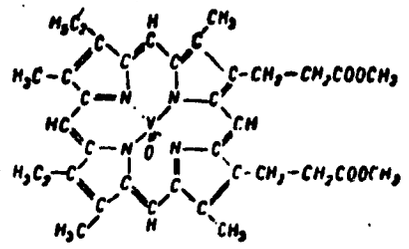

Fig. 3. Molecular structure of the compound vanadium porphyrin.

results in the high corrosion rates.

Experiments have shown that vanadium is present in petroleum in the form of a metallic compound that is soluble in it – vanadium porphyrin (Fig. 3). The vanadium contents in the petroleum and in the ash are listed in the table.

1 Место добычи нефти	2 Количество ванадия в нефти, %	3 Количество ванадия в полученной золе, %
4 Венесуэлла	0,025	75
5 Средний Восток	0,003	8
6 Оклахома	0,005	22
7 Техас	0,0002	1,4

1) Place of origin of petroleum; 2) quantity of vanadium in petroleum, %; 3) quantity of vanadium in ash formed, %; 4) Venezuela; 5) Far East; 6) Oklahoma; 7) Texas.

In addition to V_2O_5, the fuel ash also contains other oxides that are also powerful oxidation factors (66.6% V_2O_5; 8.7% NiO; 12.8% SO_3; 5.2% Na_2O; 1.8% Fe_2O_3; 1.5% Al_2O_3; 0.8% CaO; 1.3% – other constituents) [8].

Schlaepfer, Amgwerd and Preis [8] showed that certain vanadium-bearing oil ashes accelerate the formation of scale considerably on hot-strength steels and that the alkali-component content in the ash also influences the extent of deterioration.

This deterioration is so considerable that gas turbines operating on low-grade oils may be used only in those practical cases in which the blade temperature does not exceed 550°.

Bucher [15] investigated several types of stainless steels as

materials for gas-turbine blades for operation in fuel oil. He observed intensified deterioration, which did not occur when a petroleum that did not contain vanadium compounds was fused. Bucher's experiments showed that an alloy with a high nickel content (Nimonic 80) is rather resistant to accelerated oxidation.

Extensive investigations were carried out by Amgwerd [7] and Evans [10] on the deterioration of certain steel types used in the USA and other countries on exposure to the ash of low-grade petroleums. It was shown that corrosion by fuel-oil ash is more intensive than that occuring on contact with V_2O_5 alone. The rate of corrosion breakdown increased sharply with increasing temperature.

Subsequently, Brasunas and Grant [12] studied the influence of mixtures of various oxides on corrosive deterioration of several types of materials.

Below we list these oxides and their melting points in °C:

V_2O_5	670		
MoO_3	795	V_2O_5—MoO_3*	720—610
Bi_2O_3	820	V_2O_5—PbO*	—
KF	880	V_2O_5—Bi_2O_3*	—
PbO	880	V_2O_5—WO_3*	—
WO_3	1473	V_2O_5—NiO*	1275—635

It was found that the oxides and oxide mixtures with the highest melting points produce the least pronounced destructive effects (WO_3, V_2O_5 – WO_3, V_2O_5 – NiO).

In 1952, Brasunas and Grant [13] conducted extensive and detailed investigations of the scaling resistance of alloys with various contents of carbon, chromium, nickel, molybdenum, silicon, manganese and vanadium in the presence of V_2O_5 and MoO_3.

The oxidation was effected with vapors of the oxides V_2O_5 and MoO_3 and with the fused oxides. It was found that the damage done by the gaseous oxide MoO_3 was more intensive than that due to the gaseous V_2O_5. On the other hand, the action of these oxides in the molten

state was considerably stronger than that of pure oxygen.

Since severe damage to the alloys is due to the surface formation of low-melting compounds consisting of the oxides, we determined the melting points of combinations of the oxides V_2O_5 and MoO_3 with Fe_2O_3, NiO and Cr_2O_3. The melting points (or decomposition temperatures) of these compounds were found to be as follows (°C):

MoO_3—Cr_2O_3	1000
MoO_3—NiO	1330
MoO_3—Fe_2O_3	875
MoO_3—V_2O_4	760
V_2O_5—3NiO	1275
V_2O_5—Fe_2O_3	815
V_2O_5—Cr_2O_3	—

As will be seen from these figures, the melting points of combinations containing nickel oxide are rather high; this is in agreement with the rather satisfactory scaling resistance of nickel-base alloys.

Garris [16] made extensive investigations to ascertain the influence of the composition of gas-turbine alloys on their resistance to scaling and deterioration in the presence of V_2O_5.

None of the alloys investigated, which were based on cobalt, nickel, chromium or iron, was found resistant to deterioration in the presence of V_2O_5; this applies particularly to the iron-base alloys and temperatures above 750°. Such alloying additives as molybdenum, vanadium, niobium and titanium had no particularly detrimental effect on the high-temperature corrosion resistance of these alloys.

Certain authors [17] investigated the oxidation resistance of nickel-chromium alloys and stainless steels in V_2O_5 and mixtures of the latter with Na_2SO_4. It was found that the nickel-chromium alloys are more resistant than the stainless steels, and that molybdenum steels deteriorate very rapidly.

Actually, the corrosive effect of the medium is more complex due to the presence of sulfur, which is also an important factor in deterioration of the materials [18].

Subsequent research into the corrosive effect consisted in searching for additives to the alloys that would form nonreactive stable compounds with V_2O_5. It was assumed that normal vanadates of the type $MeVO_4$ would serve as such additives.

Lukas [19] ran experiments in which V_2O_5 oxidized alloys with a chromium additive (iron – chromium, cobalt – chromium, nickel – chromium). The alloy most resistant to deterioration was found to be that based on nickel. The chromium vanadate that formed was not, however, stable in the presence of chromium ions. Thus, the protective properties of the Cr_2O_3 film are lost in the presence of V_2O_5 as a result of the formation of unstable chromium vanadates.

Consequently, attempts to find a heat-resistant alloy capable of withstanding catastrophic oxidation by V_2O_5 were not crowned with success. But all of these alloys with high nickel contents were found more resistant to the corrosion than alloys not containing nickel, although their resistance to deterioration is still much weaker than that required for operation of turbines.

Na_2SO_4 In Gas Turbines

As we know, Na_2SO_4 is an undesirable ash component that forms during operation of certain powerplants.

The part played by alkali sulfates in the corrosion of steam-boiler tube walls was first described in detail by Corey, Cross and Reid [20], who observed deterioration of low-carbon steels at temperatures no higher than 400 – 500°.

In gas turbines that burn petroleum residues, the formation of Na_2SO_4 is of great importance because the ash may be deposited directly on the working surfaces. These deposits reduce the gas-flow section and give rise to corrosive deterioration of the turbine's materials.

It would hardly be expected that Na_2SO_4 itself would vigorously attack heat-resistant alloys; perhaps the alloy reacts with Na_2SO_4 to form a small quantity of low-valence sulfur. Such sulfur is more reactive than Na_2SO_4.

Sykes and Shirley propose [21] that the petroleum does not contain Na_2SO_4. It is assumed that this salt forms during combustion with a reaction somewhat as follows:

$$2NaCl + (-S) + 2(-H) + 2O_2 = Na_2SO_4 + 2HCl.$$

Since low-grade petroleum contains much sulfur, the quantity of Na_2SO_4 in the ash is determined solely by the sodium content in the fuel [22].

By virtue of the low melting point (883°), Na_2SO_4 affects the physical properties of the ash considerably.

The presence of Na_2SO_4 assists in depositing ash from the turbine's working surfaces, influences the compactness of the deposit by sintering it, influences the residence time of the deposit in the adsorbed state on the surfaces, affects the thickness of the deposit and the type of surface created as a result of the deposition, which affects the speed of the moving gas flow.

Satz [22] was the first to note that Na_2SO_4 may have a serious influence manifested in corrosion of heat-resistant alloys. He confirmed that the sulfur present in the sulfide inclusions around the mercury tubes of steam boilers which come into contact with the flame was produced from Na_2SO_4. This was corroborated by Sykes and Shirley [22], as well as by the results of numerous "crucible tests" run by Buchland, Gardiner and Sanders [23]. In these studies, several alloys were heated in contact with various mixtures that had been formed in gas turbines on combustion of fuel residues.

The results of these tests made with Na_2SO_4 were frequently

found to be ambiguous; in some cases, no deterioration was observed, while in others the material disintegrated completely.

Severe deterioration was usually observed in cases when the Na_2SO_4 was contaminated by carbon. The sulfate was obviously reduced to pure sulfur by the carbon. On the other hand, the sensitivity of the heat-resistant alloys to sulfur and certain sulfur compounds (with the exception of sulfates) is a well-known fact [24].

Literature data concerning the part taken by Na_2SO_4 in breaking down various materials are contradictory. To account for these contradictions, Simons and Browning [25] undertook a series of researches on the deterioration of steel 310 at 950° by fused Na_2SO_4 and thin films of it. They observed severe deterioration of the material, and, in their opinion, this was accelerated both by breakdown of the protective film and by an increase in temperature resulting from an exothermic reaction, as well as formation of a low-melting eutectic of the metal and its sulfide. This takes place in accordance with the following scheme.

1. Initial reduction of Na_2SO_4 by some reducing agent:

$$Na_2SO_4 + 3R = Na_2O + 3RO + S.$$

2. Reaction of the low-valence sulfur with steel to form the sulfide:

$$M + S = MS.$$

3. Autocatalytic decomposition:

$$Na_2SO_4 + 3MS = 4S + 3MO + Na_2O;$$
$$4M + 4S = 4MS;$$
$$M + MS = M \cdot MS - \text{eutectic};$$
$$M \cdot MS + O = MO + MS.$$

Thus, accelerated oxidation is due to the formation of a low-melting eutectic from the metal and the metal sulfide, which may penetrate through the protective film into the metal and propogate

rapidly along the boundaries of its grains.

I.N. Frantsevich [26] stated that active decomposition of gas-line tubing is produced by the formation of low-melting sulfide eutectics (melting points 600, 900°) of iron, ferrous sulfide and nickel with a solid β-solution, as well as from the sulfides and oxides of these elements.

Accelerated oxidation due to low-valence sulfur was observed by Preece et al. [27] in extensive investigations on scaling of low-alloy steels in a furnace atmosphere.

In such an atmosphere, the presence of SO_2 leads to rapid oxidation of steel. This oxidation is accompanied by intergranular penetration of the iron-sulfide eutectic into the metal.

Skinner [28] reported similar accelerated oxidation of heat-resistant alloys in an atmosphere containing small quantities of sulfur, and accounted for this by the formation of low-melting sulfide eutectic.

Sulfates and Chlorides in Fuel Ash

In 1949, rapid deterioration of overheated chromium-nickel steel (25% Cr, 20% Ni) holders was observed to occur in steam boilers

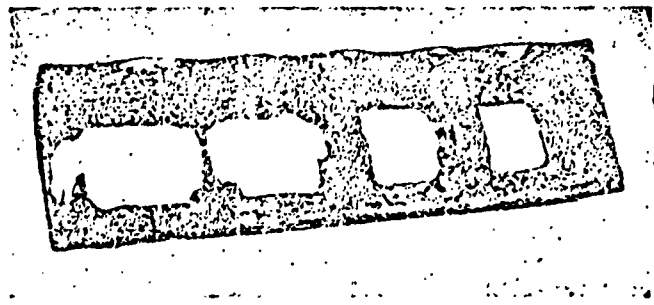

Fig. 4. Chrome-nickle steel (25% Cr, 20% Ni) covered with crust.

as a result of heavy contamination of the fuel oil by sea water containing Na_2SO_4 (Fig. 4). The most rapid corrosion was observed at

850 - 900°, but it has not yet been established in this case whether small chloride additives had any influence. Reference [18] gives information on the deterioration of various steels in contact with Na_2SO_4 contaminated with 0.3% of NaCl during a 500 -hour period. While The Na_2SO_4 itself had little influence on the rate of scaling, the introduction of chlorides produced a sharp increase in the corrosion speed.

At the present time, this danger is overshadowed by the "vanadium" problem. Investigations carried out with oils that do not contain vanadium have shown that this problem requires careful study; in particular, peat-ash deterioration of the equipment of certain gas turbines has shown that under certain conditions, steels and nickel-based alloys are considerably affected by this form of attack.

Shirley [31] investigated the influence of composition and temperature of a number of mixtures of sulfates and chlorides of sodium and calcium on various heat-resistant materials (HR-steel and nickel-base alloys). The authors of [31] conclude that here we observe the reduction of Na_2SO_4 to the sulfide of the metal, which is what causes the sharp deterioration of the materials. These conclusions are consistent with the reasoning of Simons and Browning [29] concerning the role of the sulfides formed in the process of catastrophic oxidation of the alloys.

Protection from Attack

The use of vanadium and molybdenum as alloying additives in heat-resistant alloys and the use of raw oils containing vanadium as fuels for gas turbines, steam boilers, diesels and other high-temperature equipment require not only a fuller understanding of the mechanism by which heat-resistant alloys become subject to accelerated oxidation, but also the determination of ways to eliminate it.

Catastrophic oxidation has been extensively studied over the last eight years. Several methods have been found to control it.

The role of fuel additives containing vanadium

During combustion of liquid-fuel residues, slags that accumulate in the nozzles form from the elements that are present in the fuel and corrode the metallic parts. Such accumulations of slag components in the gas passages of turbines reduce their power and efficiency. It has been found that about 2 tons of ash pass through a turbine when it is operated at full load for 1000 hours. Since the first phase of the nozzle cannot accumulate more than 400 – 1000 g of ash without a considerable loss in power and efficiency, it is natural that deposits of this type represent a serious danger. There are three possible ways to reduce this type of damage: 1) selection of corrosion-resistant materials; 2) the use of surface coatings on the metals and alloys; 3) the use of various fuel additives to render the ash passive as regards corrosion. The problem of reducing the aggressiveness of fuel has been the subject of a large number of studies. It has been proposed that a simple solution of the accelerated-oxidation problem may be achieved by adding compounds to the oil or gas flow that influence the physical properties of the ash, reducing its adhesiveness, or by combining ash elements (Na, SO_3, Na_2O, Fe_2O_3, Al_2O_3, CaO, V_2O_5) into high-melting stable compounds.

Many useful additives (high-melting oxides and the corresponding metals) have been tested to find ways of eliminating corrosion and effectively breaking up the deposited phases, but the alkaline-earth metals have been found most effective.

Monkmann [14] investigated the influence of various additives (CaO, MgO and NiO) on the corrosion resistance of certain heat-resis-

tant steels to synthetic fuel ash. The vanadium-containing synthetic ash had the following composition (according to Evans): 60% V_2O_5; 15% Na_2SO_4; 10% CaO; 5% SiO_2; 5% Fe_2O_3; 5% PbO.

The approximate melting points of such an ash diluted with increasing quantities of MgO, CaO, NiO, ZrO_2, Cr_2O_3, TiO_2, ZnO, Al_2O_3 and SiO_2 were determined.

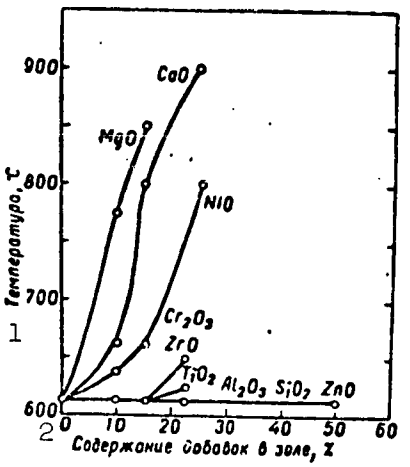

Fig. 5. Influence of additives of various oxides on melting point of ordinary liquid-fuel ash. 1) Temperature, °C; 2) additive content in ash, %.

It will be seen from Fig. 5 that MgO, CaO and NiO raise the melting point of the ash considerably, while Al_2O_3, ZnO and SiO_2 affect it only insignificantly even when diluted with 50% of the ash; ZrO_2, Cr_2O_3 and TiO_2 raise the melting point only very slightly. Since CaO, MgO and NiO raise the melting point of the ash markedly when the ash contains about 60% V_2O_5, they may serve as a means of controlling accelerated oxidation of stainless steels.

Certain authors [29] have even proposed a fuel specification that defines the content of ash components in the fuel. According to this specification, calcium was used as an oil additive to eliminate corrosion caused by V_2O_5, and the sodium-to-calcium ratio in the ash necessary to eliminate deterioration due to sodium sulfate was regarded as equal to or smaller than 0.3. Bukland made a detailed investigation of the manner in which elimination of various components of the oil influences the corrosion resistance of the material [29].

Centrifuging of the oil with certain salt solutions removed calcium, sodium and other components. Figure 6 shows the influence

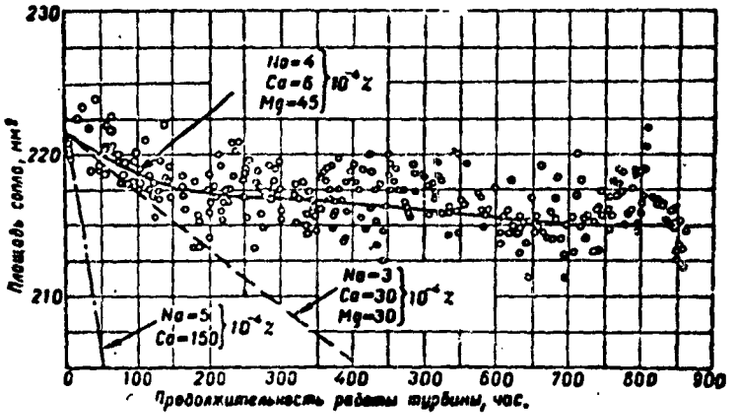

Fig. 6. Influence of elimination of sodium and calcium on formation of deposits in gas-turbine nozzle. 1) Nozzle area, mm^2; 2) operating time of turbine, hours.

of removal of sodium and calcium from the oil on accumulation of ash. Calcium is usually a corrosion inhibitor for the corrosion due to V_2O_5, but since it produced large deposits, it was desirable to eliminate it as well. Magnesium, which did not produce deposits, was used as the corrosion inhibitor; if deposits did form, they formed in very small quantities. Figure 7 shows the influence of various additives to a fuel containing 0.035% V on the corrosion resistance of chromium-nickel alloy (25% Cr, 20% Ni).

Calcium and magnesium additives were found to be most effective. A detailed study of the influence exerted by various additives (MgO, Al_2O_3, ZnO, diatomaceous earth) on the corrosion rate of a heat-resistant alloy based on nickel was conducted by Frederick and Eden [30]. It was found that the Al_2O_3, diatomaceous earth and vermiculite additives increase the rate of deterioration considerably if the additives are present in certain critical proportions (Fig. 8, b, c and d). In the case of MgO, no such relationship was observed (Fig. 8a). It has not yet been definitely established whether the reduction in corrosion is a result of formation of

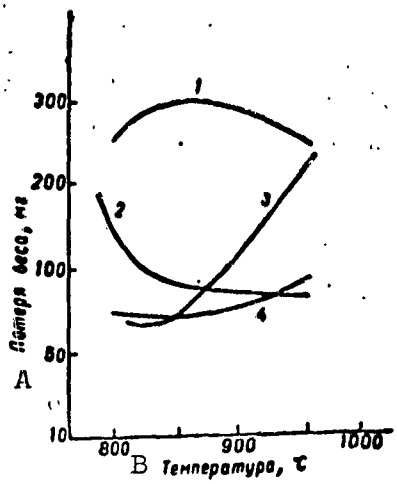

Fig. 7. Influence of additives on corrosion of chromium-nickel steel (25% Cr, 20% Ni) by a liquid fuel containing 0.035% V. 1) Raw oil; 2) calcium; 3) magnesium; 4) calcium and magnesium. A) Weight loss, mg; B) temperature τ.

inert compounds between the additives and V_2O_5 or of the removal of the ash mixtures from the zone of contact with the metallic surface by way of adsorption. It is assumed that in the case of ZnO and MgO, certain chemical compounds are formed, while the Al_2O_3, SiO_2 and vermiculite act chiefly as adsorption solvents.

SO_3 in gas turbines

In operation of gas turbines at temperatures of the order of 650°, favorable conditions are set up for increased sulfatation of the basic

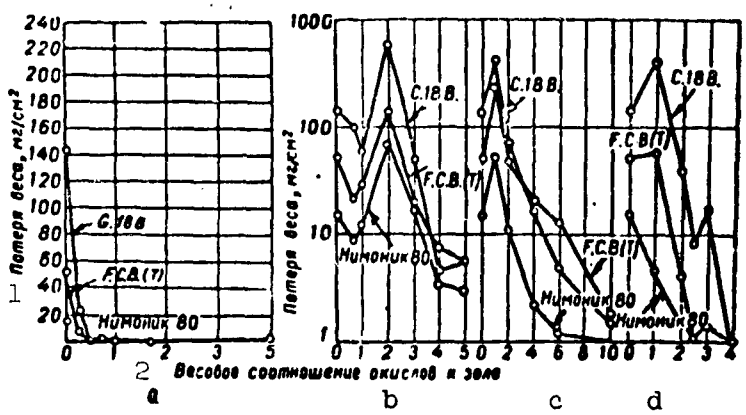

Fig. 8. Influence of various additives on scaling of certain alloys at 700°. Ash composition 90% V_2O_5 + 10% Na_2SO_4. 1) Weight loss, mg/cm²; 2) nimonic 80; 3) weight ratio, oxides to ash.

additives (oxides). The presence of SO_3 is the most serious factor causing deterioration of scaling resistance and low temperatures.

It is known that SO_3 reacts with the basic oxides MgO, ZnO and Al_2O_3, causing breakdown of their chemical activity. The decay temper-

ature of the sulfate indicates the upper limit about which this sulfatation may be observed ($MgSO_4$ – 890°; $ZnSO_4$ – 720°; $Al_2(SO_4)_3$ – 590°).

Thus, if sulfatation of the basic oxides actually reduces their effectiveness to a considerable degree, we must either select compounds that suppress the formation of SO_3 or use additives that are not subject to decomposition in its presence.

Conclusions

1. The presence of vanadium, sulfur and alkali components in a fuel, which produce V_2O_5, Na_2SO_4 and Na_2S on its combustion, is an important factor leading to catastrophic damage to gas turbines.

2. At temperatures in excess of 650°, corrosion takes place at a tremendous speed as a result of formation of low-melting compounds or eutectics from the oxide forming the ash (V_2O_5, Al_2O_3, CaO) and oxides of the initial material.

3. The damage caused by Na_2SO_4 is obviously governed by its reduction to Na_2S with formation of a metal-sulfide eutectic that penetrates through the protective oxide film on the metal and propagates along its grain boundaries. Metal dissolved in this manner in the eutectic becomes exceptionally reactive.

4. Na_2SO_4 lowers the melting point of V_2O_5 and thereby contributes to more rapid breakdown of the material.

5. Mixtures of alkali-metal sulfates and chlorides present in the fuel cause considerable deterioration, evidently as a result of the appearance of low-valence sulfur (sulfides).

6. Of the materials of the types studied, the most resistant to oxidation by liquid-fuel ash are nickel-based alloys, since in this case relatively high-melting compounds form from the oxides of nickel and the oxides forming the ash.

On the other hand, in the presence of sulfur-containing substances, nickel alloys lose these properties as a result of the formation of a low-melting (645°) metal-sulfide eutectic, which penetrates through the oxide film and breaks the metal down in this way.

7. Alloys with alloying additives such as vanadium, molybdenum and tungsten, whose higher oxides have low melting points, are subject to rapid oxidation in air.

8. The use of various fuel additives that form high-melting stable compounds may take us somewhat closer to a solution of the problem posed by accelerated deterioration of the materials due to attack by liquid-fuel ash, as may the use of enamel-type coatings.

REFERENCES

1. W.C. Leslie, M.G. Fontana, Trans. Am. Soc. Metals, 41, 1213. 1949.
2. E. Scheil, Z. f. Metalkunde [J. for Physical Metallurgy], 29, 209, 1937.
3. B. Lystman, "Metal Progress", 57, 5, 629, 1950.
4. I.K. Meijering, I.W. Rathenau, "Nature", 165, 240, 1950.
5. A. Preece, Iron Steel Inst. Spec. Report, N 43, 149, 169, 1951.
6. E. Fitzer, J. Schwab, Berg. Huettenmann Monatshefte [Min. Met. Monthly], 98, 1, 1953.
7. P. Amgwerd, Doctor's thesis Eidgenossischen Technischen Hochschule in Zuerich [Confederation Technical High School, Zuerich], 1949.
8. Schlaepler, P. Amgwerd, H. Preis, Schweizer Archiv fuer angewandten Wissenschaft und Technik [Swiss Arch. Appl. Sci. and Tech.], N 10, 29, 1949.
9. P.F. von Sulzer, Schweizer Archiv [Swiss Arch.] N2, 33, 1954; W.L. Nelson, Oil Gas J., 49, N 30, 88, 1950; N 31, 104 - 106,

1950; N 33, 330, 1950; N 34, 83, 1950, 50, N. 35, 651, 1951.

10. C.T. Evans, Symposium on corrosion of Gas turbine Materials at elevated temperatures, Spec. Tech. Publication, N 108, A.S.T.M., 1950.
11. J. Piert, R. Scheidegger, Schweiz Archiv angew., Wiss. u. Tech., 19, N 12, 309 - 366, 1953.
12. A. des Brasunas, N.I. Grant, Iron Age, 166, 85, 1950.
13. A. des Brasunas, N.I. Grant, Trans. Am. Soc. Metals, 44, 1117, 1952.
14. F.C. Monkmann, N.J. Grant, "Corrosion", 12, 461, 1953.
15. I.B. Bucher, Trans. Am. Inst. Eng. and Shipbuilders. in Scotland, paper 1125, 1950.
16. G.T. Garris, H.C. Child, I.A. Kerr, I. Iron Steel Inst., 179, 241, 1955.
17. W. Betteridge, K. Sachs, I. Inst. Petroleum, 41, 170, 1955.
18. S. Sykes, H.T. Shirley, Symposium on high temperature Steels and alloys for Gas turbine, Iron Steel. Spec. Report, No. 43, 153, 1951.
19. W.C. Reid, M. Weddle, A. Preece, I. Iron Steel Inst., 179, 342, 1955.
20. W.C. Reid, R.C. Corey, B.J. Cross, Trans. Am. Soc. Mech. Eng., 67, 279, 289, 1945.
21. S. Sykes, H.T. Shirley, Iron and Steel Inst. Spec. Report, No. 43, 153, 1952.
22. H.R. Berry, Report to Oil ash corrosion comittee of Mercury Boiler owners and manufacturers (quoted by L.H. Satz, General Electric Report, D.F. 505 L. 305. Sept. 28, 1952).
23. B.O. Buchland, C.M. Gardiner, D.M. Sanders, paper A-52-161, annual meeting of Am. Soc. Mech. Eng. New York, December, 1952.

24. O. Kubaschewski, O. von Golbdeck, Metalloberflaeche [Metal Surface], 8, A33, 1954.

25. E.L. Simons, G.V. Browning, H.A. Liebhafsky, "Corrosion", 11, 17, 1955.

26. I.N. Frantsevich, Ye.A. Bilenko and R.B. Malashenko, Collected Papers of Institute chernoy metallurgii AN USSR [Inst. Ferrous Metals Acad. Sci. UkrSSR], 1, 84, 1946.

27. A. Preece, G.T. Richardson, I.W. Cobb. E. "Simister Iron Steel Inst. spec. Report, No. 24, 9, 1939; A. Preece, K.I. Irvine, I. Iron Steel Inst., 157, 336, 1947.

28. E.N. Skinner "Corrosion", 12, 464, 1953.

29. B.O. Bukland, Ind. Eng. Chem., 46, 2163, 1954.

30. S.H. Frederick, H.F. Eden, "Corrosion", 11, 35, 1955.

31. H.T. Shirley, J. Iron Steel Inst., 182, 144, 1956.

32. M.G. Fontana, Ind. Eng. Chem., 42, 65 A, 1950.

Manuscript Page No.

[Footnote]

50 Mixtures consisting of 50% of each component.

COMPARATIVE INVESTIGATION OF EROSION RESISTANCE OF HIGH-TEMPERATURE CORROSION-RESUSTANT MATERIALS OF GAS TURBINES OPERATING ON SOLID FUEL

K. V. Olesevich

(Odessa Polytechnic Institute)

Introduction

Gas-turbine installations developing powers of up to 25,000 kw, which are used in stationary power engineering, have essential advantages over steam-turbine installations – they have smaller dimensions and weight (no boiler plant, no water preparation) and rather high efficiency (e.g., the efficiencies of gas-turbine locomotives run to about 18%, while those of steam locomotives are around 8%).

Despite these advantages of the gas-turbine engine, it has not yet come into wide use either in power engineering or in transportation. The reason for this is the necessity of using expensive liquid or gaseous fuels.

In operation on solid fuels, the flow-through parts of the turbine – the entrance and main blades – show rapid attrition by volatile ash in ordinary installations with an open cycle.

Existing installations in which blade attrition is excluded are well-known. The first of these is the closed-cycle installation that was proposed by Ackert and Keller and built by the firm Escher-Weiss. It was first proposed that the installation operate on all forms of fuel, including solid fuels. Thus far, however, installations

of this type are operating only on liquid fuel. The basic reason for this is apparently attrition of the heating surfaces of the air chamber and their slag formation by the volatile ash.

Our experiments showed that adhesion of the ash to specimens blasted with a gas containing ash dust is observed in many cases even when the latter is at a temperature of 550°.

In 1946, open-cycle installations in which the combustion chamber is replaced by air chambers was proposed in the USSR. Similar systems have been originated by McGill University (Canada) and the Parsons Firm (England). In all of these systems, blade attrition is supplanted by attrition of the air chamber heating surface. The danger of heating-surface attrition is well known from experience in the operation of steam boilers. Moreover, the use of air chambers increases the dimensions of the installation sharply.

Conversion of gas turbines to solid fuel involves solution of many problems. Basic among these are attrition of the flow-through section by volatile ash, preparation of the fuel, metering it and feeding it to the combustion chamber, dependable and highly efficient combustion in small combustion chambers, trapping of the ash in the combustion chamber, purification of the gases to remove volatile ash, control of the installation and so forth.

Fundamentally, all of these problems have been solved, except for the problem of countering wear on the elements of the installations — chiefly, wear of the entrance and main buckets. The TsKTI, VTI, TsNIITMASh and the Odessa Polytechnic Institute have been occupied and continue to be occupied with a study of attrition of gas-turbine flow-through elements in operation on solid fuel.

We have investigated the general qualitative laws governing attrition of surfaces blasted by dust-bearing gas. Since we were interested

in stationary power engineering, our basic attention was devoted to materials suitable for installations of this type. The tests were run at the appropriate gas temperatures and velocities. A gas temperature of 650° before the nozzle and a gas velocity of up to 500 m/sec at exit from the nozzle were taken as standard conditions.

The objective of our experiments consisted in finding wear-resistant materials. The experimental technique adopted was exceedingly simple. For convenience and clarity of presentation, a gravimetric method was employed: the specimen was blasted with the dust-bearing gas after the latter had been heated to high temperature, and the wear-resistance of the material determined from its weight loss. We had established earlier (the same results were obtained at TskTI Alferov [Central Scientific Research Institute for Boilers and Turbines, Alfers]) that the most rapid wear is observed at a 30° angle of attack. The test apparatus consisted of a combustion chamber, an accelerating tube, into which the abrasive powder was introduced, a nozzle, the test chamber, a device to trap the abrasive material behind the test chamber, and a device used to meter the latter. The specimen was weighed before and after the experiment on an analytical balance. The loss in weight per 1 kg of abrasive powder passed through served as a measure of resistance to wear.

The temperature before the nozzle was measured and that behind the nozzle was computed (the latter can also be measured, but there is no particular necessity of doing this, as we shall explain below).

The experimental technique was simple: the specimen was sent up in the test chamber at the required angle. The combustion chamber was cut in and the temperature raised to the required level. The abrasive powder was fed into the gas. The experiment was continued until the weighed portion of abrasive powder (usually 1 kg) had been

completely used up.

The specimen was weighed after the experiment. A diagram of the apparatus is shown in Fig. 1.

Ashes from various high-energy fuels were used at a temperature of 650° as the abrasive materials in our experiments; these materials were obtained by trapping them in dust extractors or electric filters at the region's major power plant.

Use of the ash was found to be impossible in tests of materials with high resistance to corrosion at high temperatures, when the gas temperature before the nozzle was 1050°; the ash softened and adhered to the specimen. In the course of time, the deposit increased, reached the nozzle and blocked it completely.

If clogging of the nozzle was not observed, the slag covered the specimen and no attrition was observed. Naturally, it would be impossible to compare the results under such conditions.

However, since the attrition resistance of the materials is an important characteristic for them, we were obliged to blast the materials with special abrasive powders, including emery powder with the following fractional composition (μ): 5.39% 53/0; 3.22% 74.53; 8.03% 105/74; 15.82% 149/105; 29.25% 210/149; 32.65% 297/210; 5.67% 420/297.

This powder composition is close to that of the ash trapped in dust extractor before exhaust fans in combustion of fuel in the dust state and granulated slag removal [sic].

Results of Experiments

Temperature of 650°. Various materials were tested. A specimen of type 18-18 austenitic steel was also tested under similar conditions for purposes of comparison. Comparative wear-resistance figures were determined by reference to the wear resistance of the austenitic

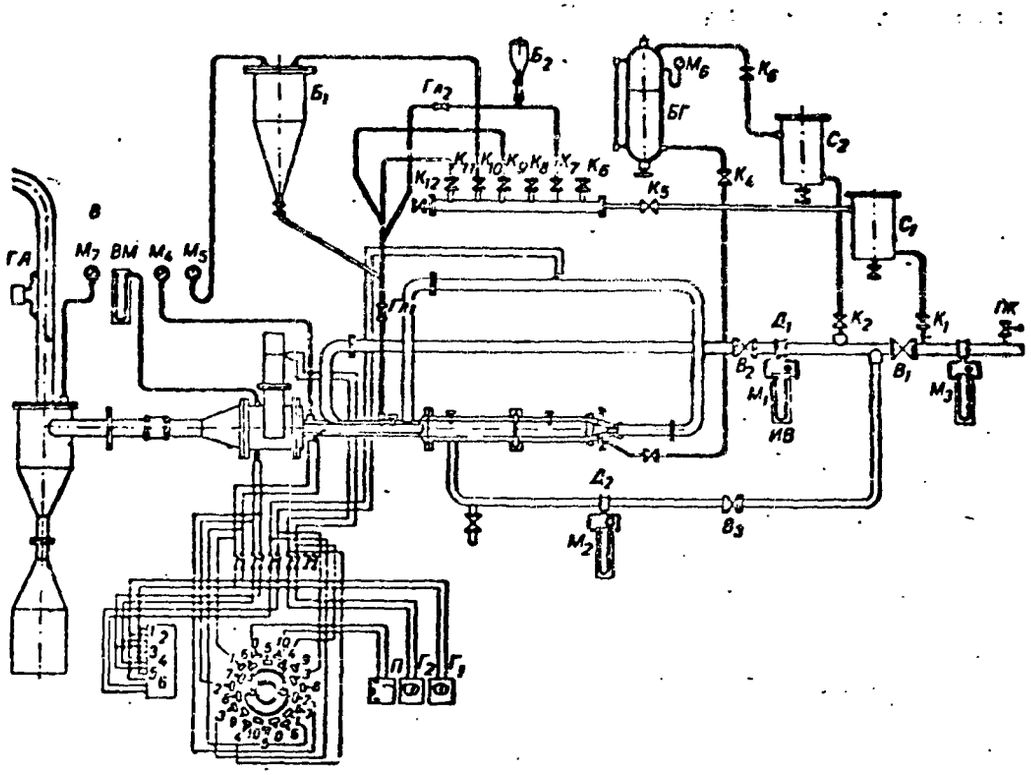

Fig. 1. Diagram of apparatus for study of attrition resistance of materials. ГА = GA; ВМ = VM; Б = B; П = P; Г = G; Гл = Gl; Д = D; БГ = BG; В = V; ИВ = IV; С = S; ПК = PK.

steel specimen.

The abrasive material was the ash of lean Donets coal; the quantity was 1000 g and the angle of attack was 30°.

The results of the experiments are presented in Table 1.

As will be seen from this table, the carbide composition, specimen No. 9, possesses the highest wear resistance. This material could be used for protection if it were possible to find a method of cementing plates to the buckets.

Specimen No. 2 was punched full of holes and its soft core was washed away.

Temperature 1050°. The experiments were run at temperatures of 1050° before the nozzle and about 925° in the test chamber. The

TABLE 1

1 Материал	2 Потеря образца в весе, г	3 Износостойкость по сравнению со сталью 18-12	4 Вид образца (рис.)	
			5 до опыта	6 после опыта
7 Сталь 18-12	0,6995	1,00		
8 Керамический образец № 1:				
9 первое испытание	0,1868	3,74		
10 второе »	0,0068*	—		
11 третье »	0,0487	14,35		
12 четвертое »	0,0313	22,30		
13 Керамический образец № 2	2,4290	0,29	2	3
14 Керамический образец № 3	0,8717	0,80		
15 Образец № 4	0,0321	21,80	4	5
16 Образец № 5	0,0753	9,30	6	7
17 Керамический образец № 6	0,1009	7,00		
18 Керамический образец № 7	0,0711	9,85		
19 Керамический образец № 8	0,0830	8,38		
20 Образец № 9	0,0025	281,0		
21 Нимоник-80	0,814	0,86		
22 Виталиум	—	0,80		
23 Микролит	0,01673	41,7		
24 Твердый сплав типа победита	0,01256	55,6		

1) Material; 2) weight loss of specimen, g; 3) wear resistance as compared to steel 18-12; 4) appearance of specimen (Fig.); 5) before experiment; 6) after experiment; 7) steel 18-12; 8) ceramic specimen No. 1; 9) first test; 10) second test; 11) third test; 12) fourth test; 13) ceramic specimen No. 2; 14) ceramic specimen No. 3; 15) specimen No. 4; 16) specimen No. 5; 17) ceramic specimen No. 6; 18) ceramic specimen No. 7; 19) ceramic specimen No. 8; 20) specimen No. 9; 21) Nimonic-80; 22) vitalium; 23) microlite; 24) hard alloy of pobedit type.

velocity of the gas at exit from the nozzle was 525 m/sec, the abrasive material was emery powder in a quantity of 1000 g, and the angle of attack 30°. The results of the experiments are listed in Table 2.

It is necessary to note that in two cases, the specimens were built up and it was impossible to determine the attrition exactly. It will apparently be necessary to repeat the experiments with elektrokorund. In actuality, the bucket assembly is not operating under such severe conditions. The sense of such tests consists in ascertaining the relative wear resistances of the materials. In operation on solid fuel and at such high temperatures, we may expect slag for-

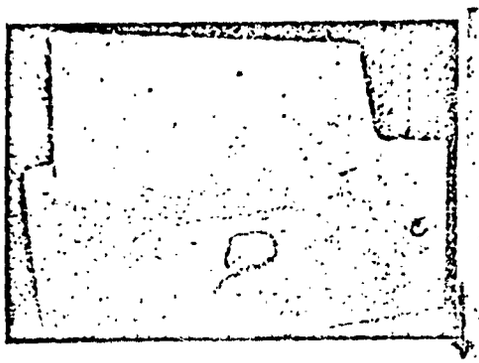

Fig. 2. Appearance of ceramic specimen No. 2 before test.

Fig. 3. Appearance of ceramic specimen No. 2 after test (temperature 650°).

Fig. 4. Appearance of specimen No. 4 before test.

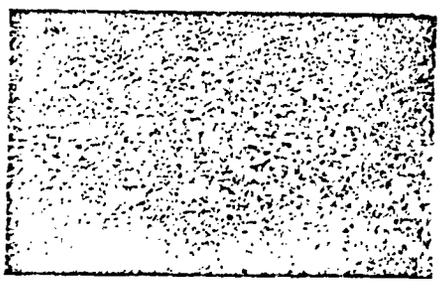

Fig. 5. Appearance of specimen No. 4 after test (temperature 650°).

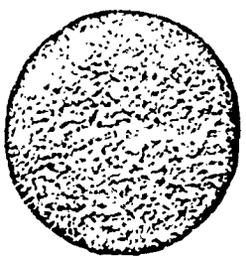

Fig. 6. Appearance of specimen No. 5 before test.

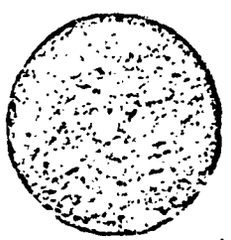

Fig. 7. Appearance of specimen No. 5 after test (temperature 650°).

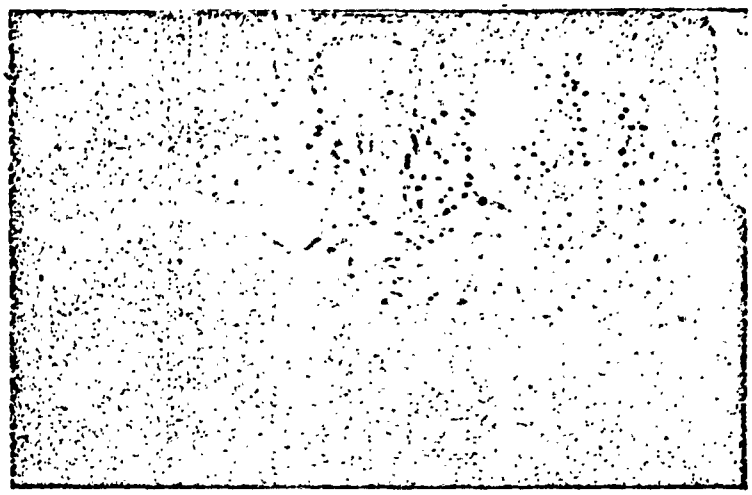

Fig. 8. Appearance of ceramic specimen No. 1 after test (temperature 1050°).

Fig. 9. Appearance of ceramic specimen No. 7 after test (temperature 1050°).

mation on the buckets, which is extremely dangerous, since it involves the same complications as are observed when salt drifts form on the flow-through parts of steam turbines. It is necessary to find materials during use of which no ash will be deposited on the bucket surfaces even in the softened state.

As concerns investigations of relative wear resistance, the seletion of abrasive here is quite arbitrary. The basic requirements in this case are the absence of slag formation and buildups over the entire temperature range of the tests and stability of the grain strength characteristics in the same temperature range. Sintered corundum will apparently be the most suitable material.

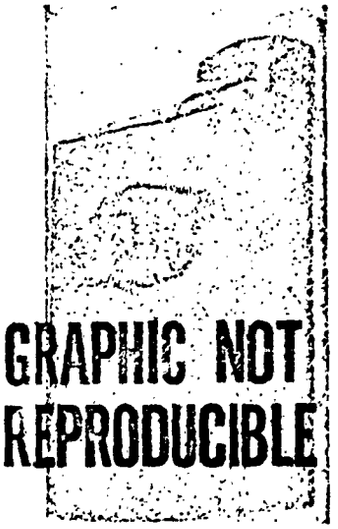

Fig. 10. Appearance of ceramic specimen No. 16 after test (temperature 1050°).

At the moment, we do not have data for comparing the wear resistances of the various materials at a gas temperature of 1050° before the nozzle. We can only state that ceramic specimens Nos. 16 – 18 show less resistance than the cermetallic specimens Nos. 10 – 15. Here, it must be remembered that the wear indices cannot be compared here, since the specific gravities of ceramics and cermetallics differ quite considerably. Our conclusions in this case are based on comparison of the depths of the pitting holes. It is sufficient to note that specimen No. 17 was perforated, and since all test specimens from No. 10 to No. 18 had the same dimensions and shape, the inadequate resistance of the ceramic specimens is obvious.

In two cases, ceramic specimens Nos. 16 – 18 had buildups of the abrasive material after the tests. This means that there are conditions

TABLE 2

1 Материалы или образцы	2 Потеря в весе, г	3 Вид образца (рис.) 4 до опыта	5 после опыта
6 Керамический образец № 1	0,5170	8	9
7 Образец № 9	0,4720		
8 Образец № 4	1,1835		
9 Образец № 10	+0,1235*		
10 Образец № 11	+0,1689**		
11 Образец № 12	0,3716		
12 Образец № 13	0,5497		
13 Образец № 14	0,7242		
14 Образец № 15	0,2668***		
15 Керамический образец № 16	+0,3789		10
16 Керамический образец № 17	0,6513		
17 Керамический образец № 18	0,2285		

1) Material or specimen; 2) weight loss, g; 3) appearance of specimen (Fig.); 4) before experiment; 5) after experiment; 6) ceramic specimen No. 1; 7) specimen No. 9; 8) specimen No. 4; 9) specimen No. 10; 10) specimen No. 11; 11) specimen No. 12; 12) specimen No. 13; 13) specimen No. 14; 14) specimen No. 15; 15) ceramic specimen No. 16; 16) ceramic specimen No. 17; 17) ceramic specimen No. 18.

that favor deposition of abrasive grains on the specimen surfaces. Such buildups are undesirable in the light of the conditions necessary to ensure dependable operation of the turbines. Finally, the results of the experiments justify the statement that the structures of the ceramic materials were nonuniform: specimen No. 1 has randomly distributed craters at the blasting point, with the soft component of the material washed out by the dust-bearing gas at these places. Such nonuniformity should be eliminated. For blades subject to ash wear, special processing affecting the entire thickness is important; creation of a protective layer on the surface alone results in intensive wear after the protective coating has been removed.

It should be emphasized further that in solving the problem of converting gas-turbine installations to solid fuel, it is necessary

to create materials that possess high wear resistance and strength not only at high temperatures, but also at moderate temperatures. The thing is that even a very high initial temperature of the gas drops rapidly in the turbine's stages as the gas expands and has reached about 650° by the third stage. Behind the turbine, the temperatures will be of the order of 400 – 450°. Since, however, the abrasive properties of the ash do not depend on pressure, attrition of the buckets is possible in early and late stages and the problem of the attrition resistance of the materials will also exist at low temperatures.

Disintegration of the abrasive particles in the first stages (on striking the buckets) reduces bucket wear to some extent in the subsequent stages, but does not eliminate it completely.

In this case, materials that can be used in the form of protective plates acquire special importance. However, methods of securing the plates to the buckets are restricted due to the high temperatures (welding-on or methods similar to enamel coating).

Manuscript Page No.

[Footnotes]

70 *During the experiment, the specimen was accidentally impregnated with grease.

74 *Ash from lean Donets coal (Odessa TETs [Thermal Electric Power Station]).

74 **Ash from Moscow brown coal (Stalinogorsk GRES [State Regional Electric Power Plant).

74 ***The abrasive material was 150 g of elektrokorund.

DISTRIBUTION LIST

DEPARTMENT OF DEFENSE	Nr. Copies
HEADQUARTERS USAF	
AFCIN-3D2	1
ARL (ARB)	1
OTHER AGENCIES	
CIA	1
NSA	6
DIA	9
AID	2
OTS	2
AEC	2
PWS	1
NASA	1
ARMY	3
NAVY	3
SPECTRUM	1
RAND	1

MAJOR AIR COMMANDS	Nr. Copies
AFSC	
SCFDD	1
ASTIA	25
TDETL	5
TDBDP	5
AEDC (AEY)	1
AFSWC (SWF)	1
SSD (SSF)	2
BSD (BSF)	1
AFFTC (FTY)	1